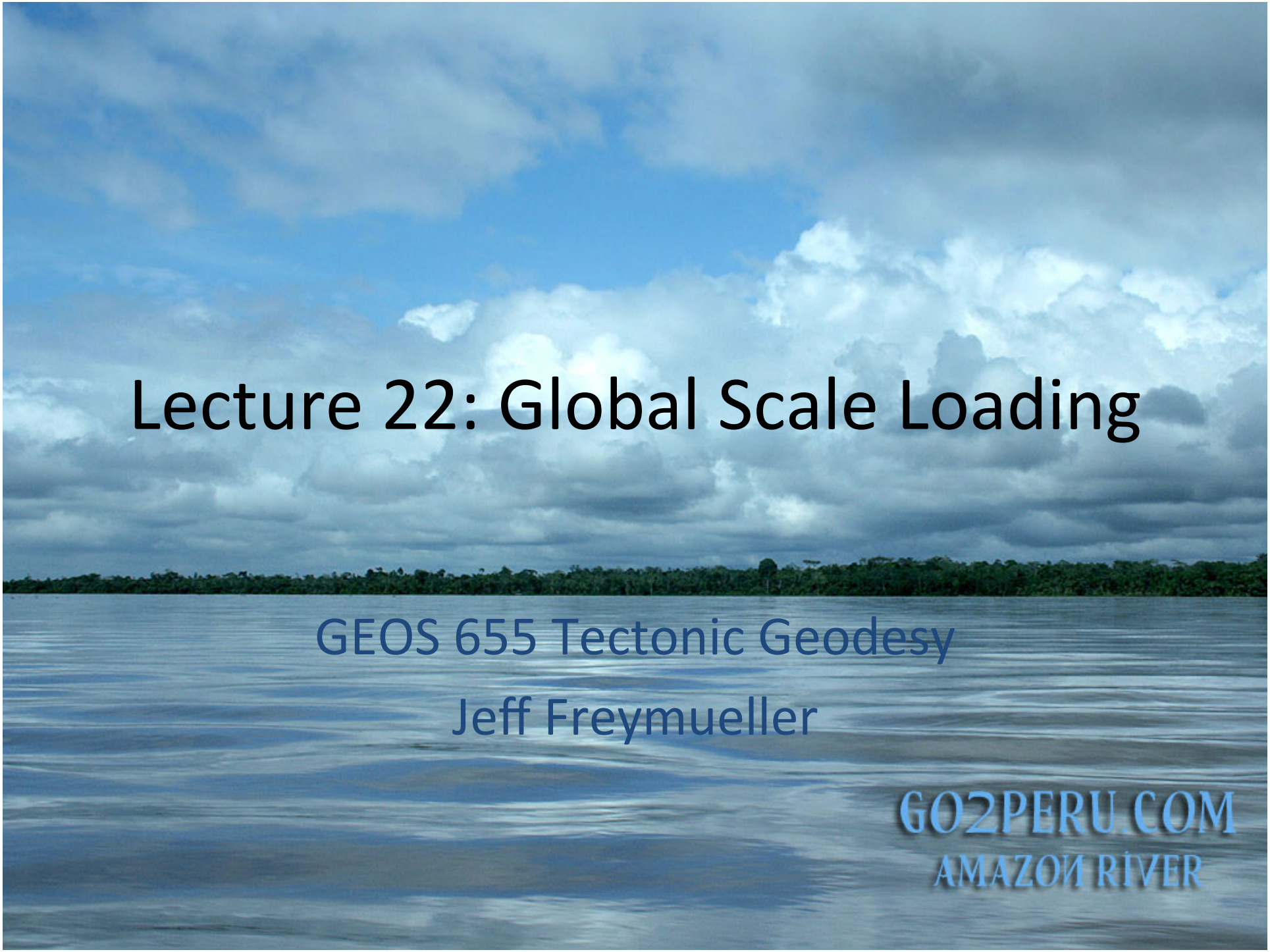

Lecture 22: Global Scale Loading

GEOS 655 Tectonic Geodesy

Jeff Freymueller

Loading Relates Gravity, Deformation

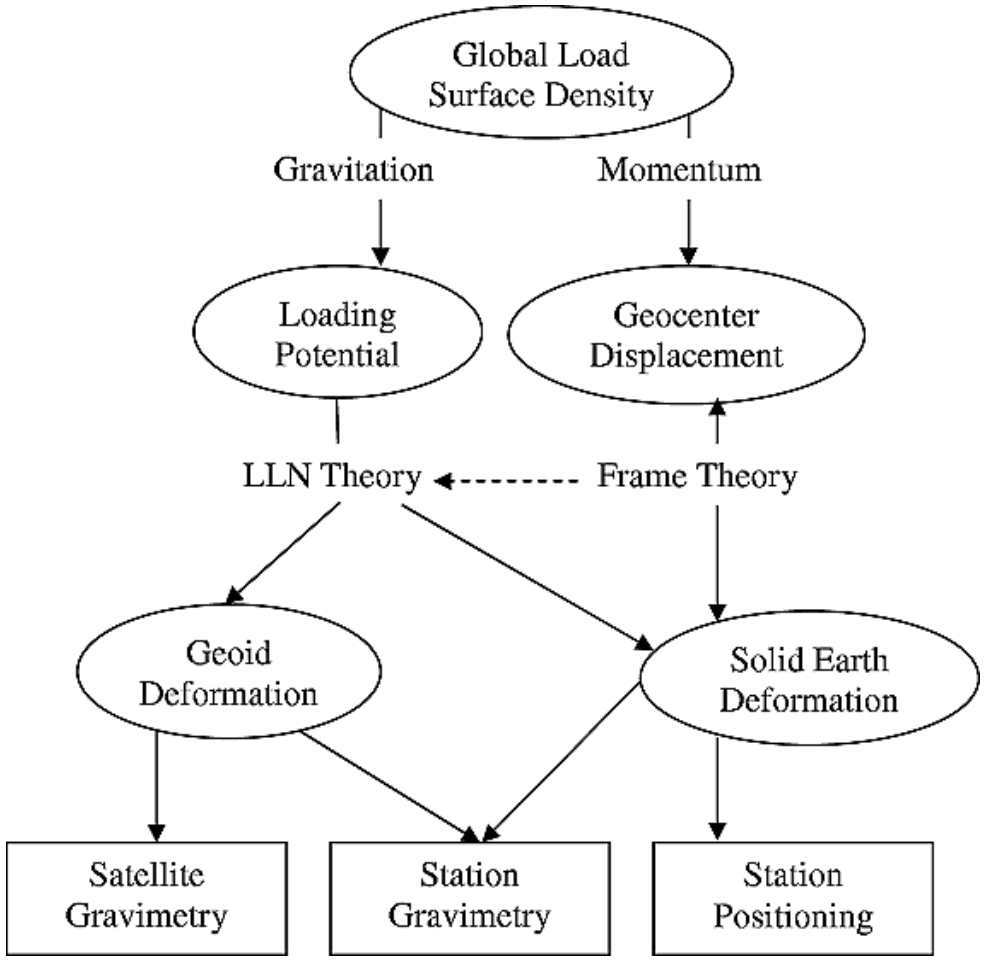

GRACE

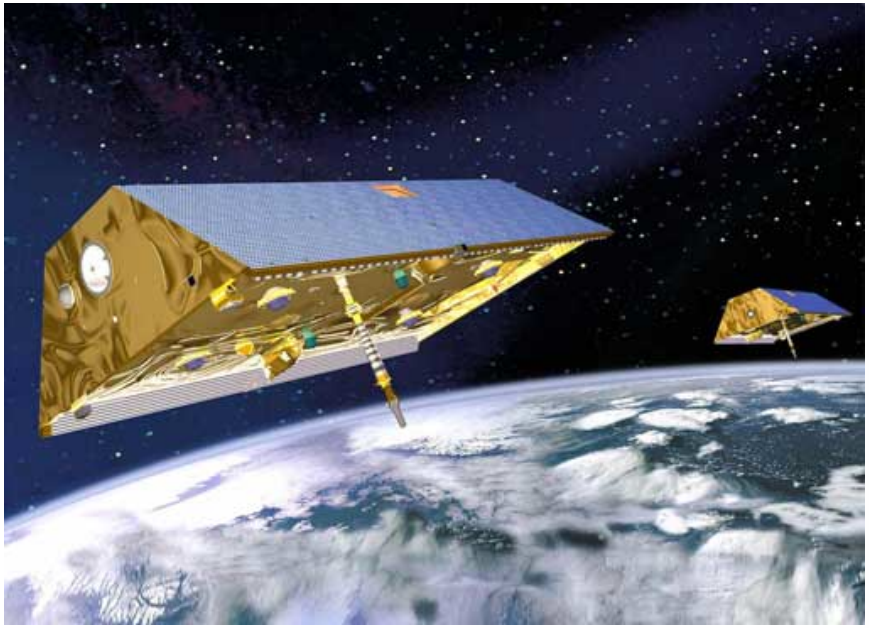

GRACE is a pair of satellites, and the key observation is the change in the distance between them, measured via a microwave ranging system.

Geoid undulations based on GRACE

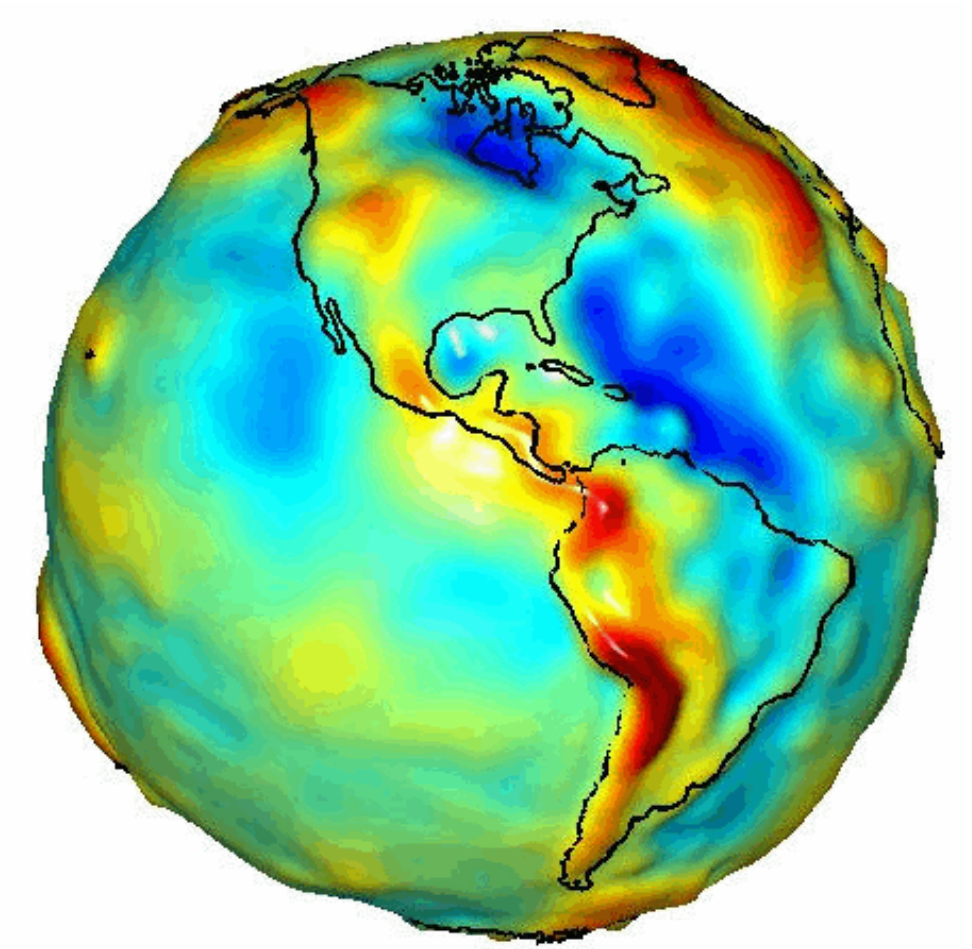

GRACE Measures Change in Gravity

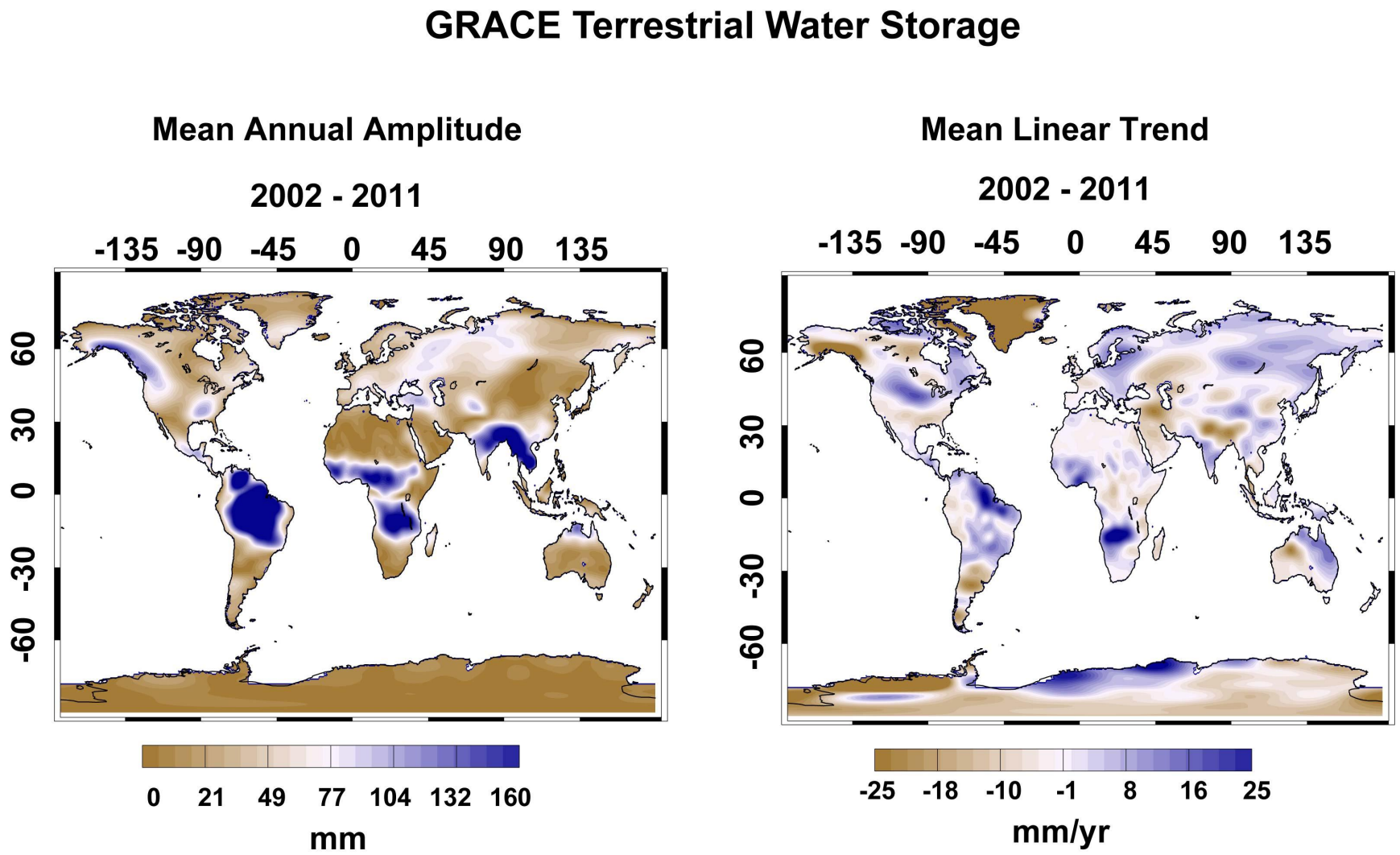

Sean Swenson, NCAR

Correlating GPS and GRACE

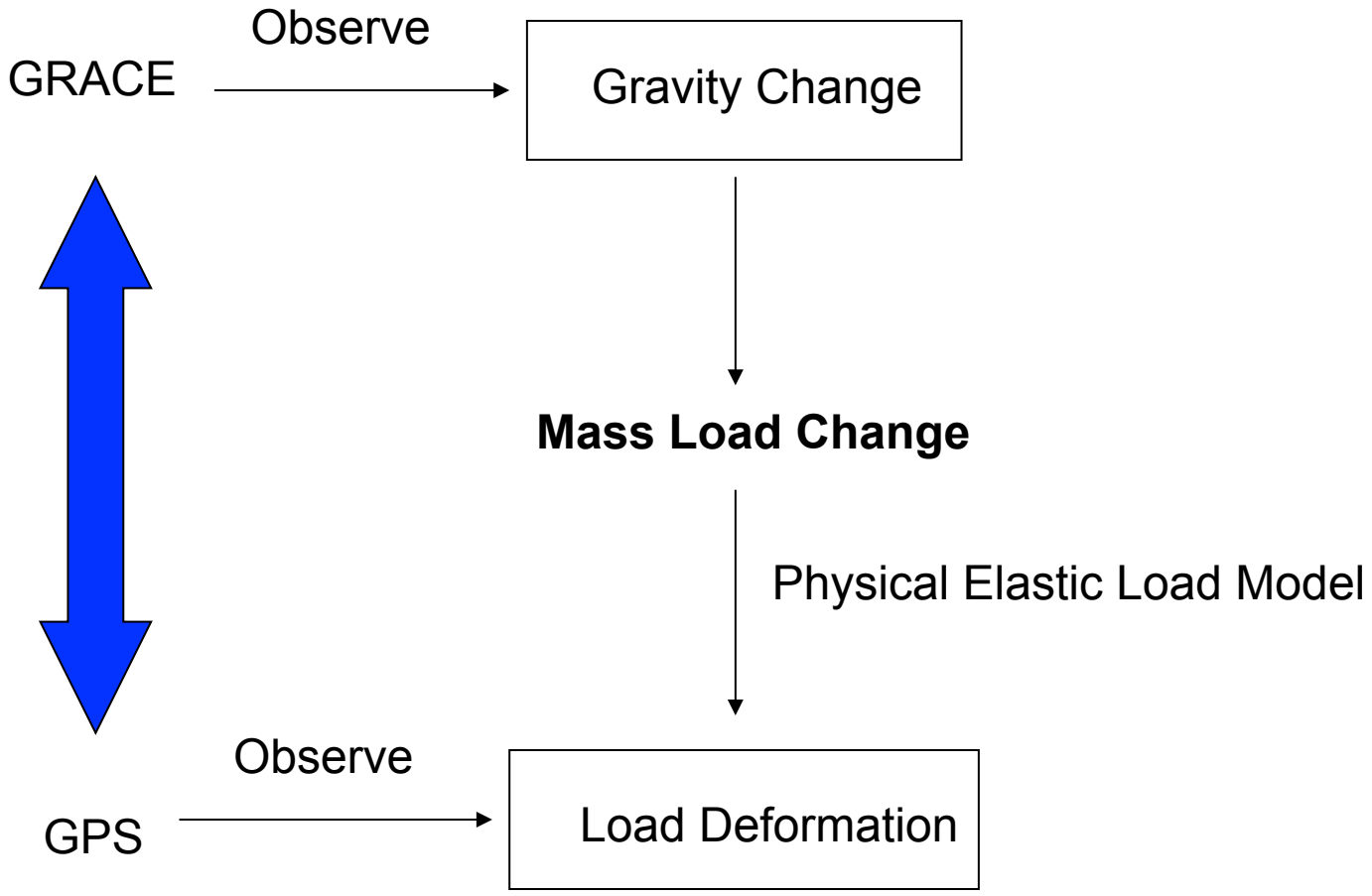

Loading on Seasonal Timescales

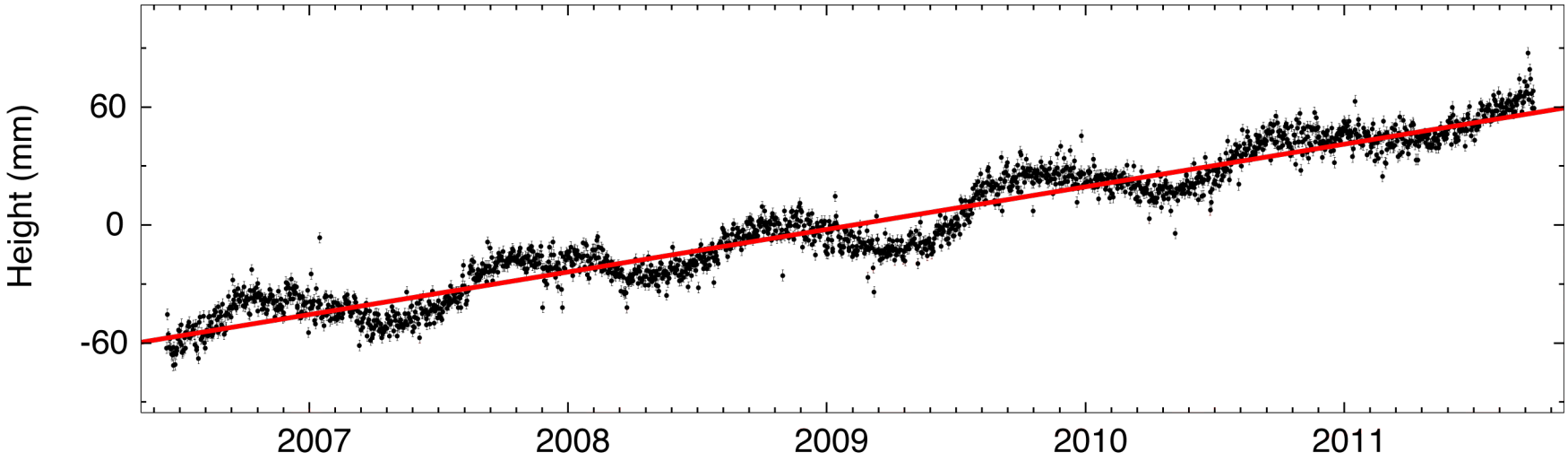

- Dominant control for seasonal/annual periods is hydrology.
- Elastic loading theory can be used to explain signal, using a load model derived from GRACE gravity change.

Elastic Model

- Spherical harmonic coefficients of the gravity field.
- Load Love numbers. [Farrell 1972]

$$\Delta h = a \sum_{l,m} \left(\Delta C^h_{lm} \cos m\lambda + \Delta S^h_{lm} \sin m\lambda \right) \overline{P}_{lm}(\cos\theta) + \mathbf{e}_h \cdot \boldsymbol{\Delta}\mathbf{x} - a\Delta s$$

$$\Delta e = \frac{a}{\sin\theta} \sum_{l,m} m \left(-\Delta C^{\psi}_{lm} \sin m\lambda + \Delta S^{\psi}_{lm} \cos m\lambda \right) \cdot \overline{P}_{lm}(\cos\theta) + \mathbf{e}_e \cdot \boldsymbol{\Delta}\mathbf{x} + \mathbf{e}_n \cdot \boldsymbol{\epsilon}$$

$$\Delta n = -a \sum_{l,m} \left(\Delta C^{\psi}_{lm} \cos m\lambda + \Delta S^{\psi}_{lm} \sin m\lambda \right) \cdot \frac{\partial}{\partial\theta} \overline{P}_{lm}(\cos\theta) + \mathbf{e}_n \cdot \boldsymbol{\Delta}\mathbf{x} - \mathbf{e}_e \cdot \boldsymbol{\epsilon}$$

$$\Delta C^g_{lm} = \frac{3\rho_w}{\rho_e} \frac{1}{2l+1} \left(1 + k'_l\right) \Delta C^{\sigma}_{lm}$$

$$\Delta C^h_{lm} = \frac{3\rho_w}{\rho_e} \frac{1}{2l+1} \, h'_l \, \Delta C^{\sigma}_{lm}$$

$$\Delta C^{\psi}_{lm} = \frac{3\rho_w}{\rho_e} \frac{1}{2l+1} \, l'_l \, \Delta C^{\sigma}_{lm}$$

[Kusche and Schrama, 2005]

Comparing GPS and GRACE

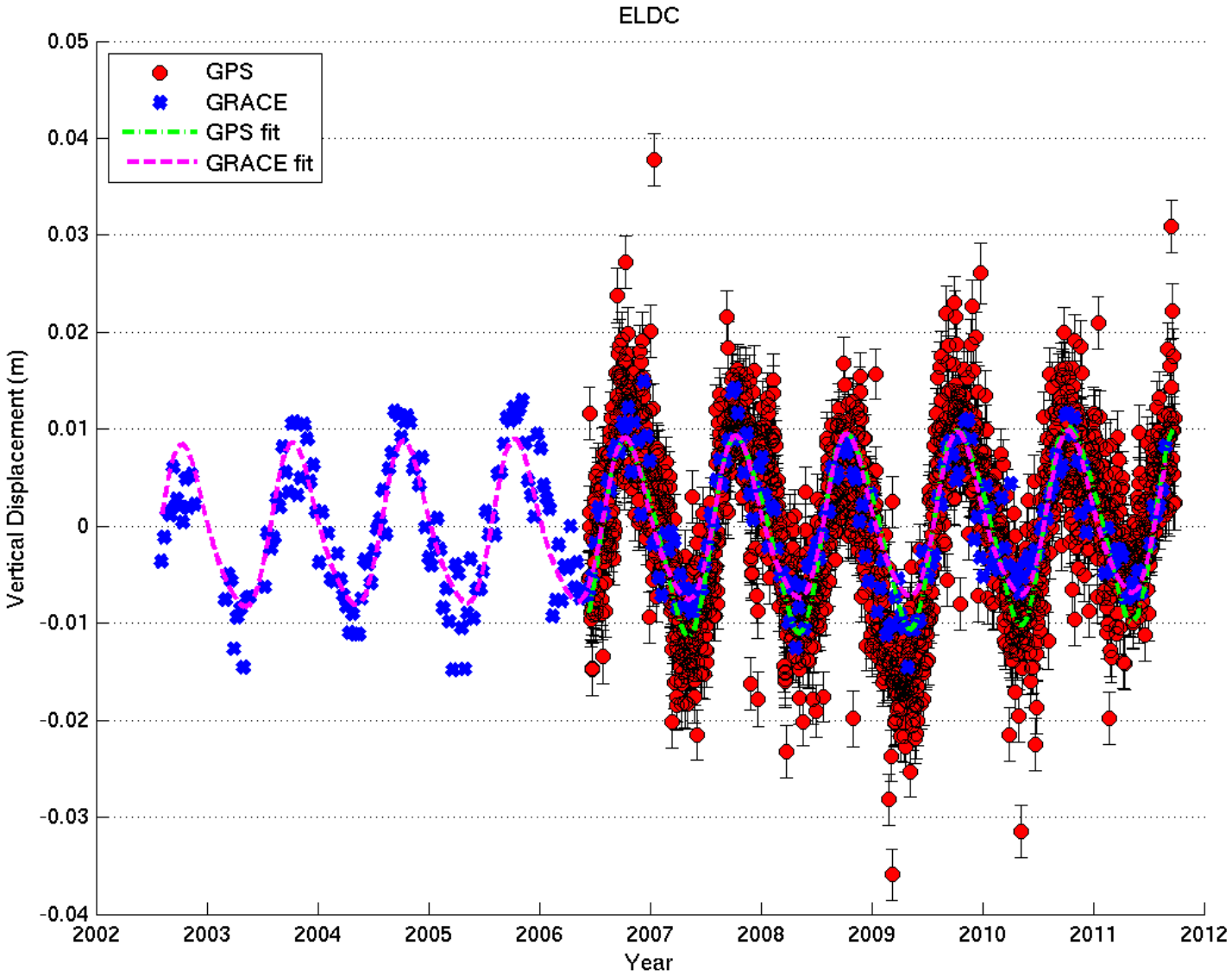

Seasonal Hydrologic Loading in Southern Alaska

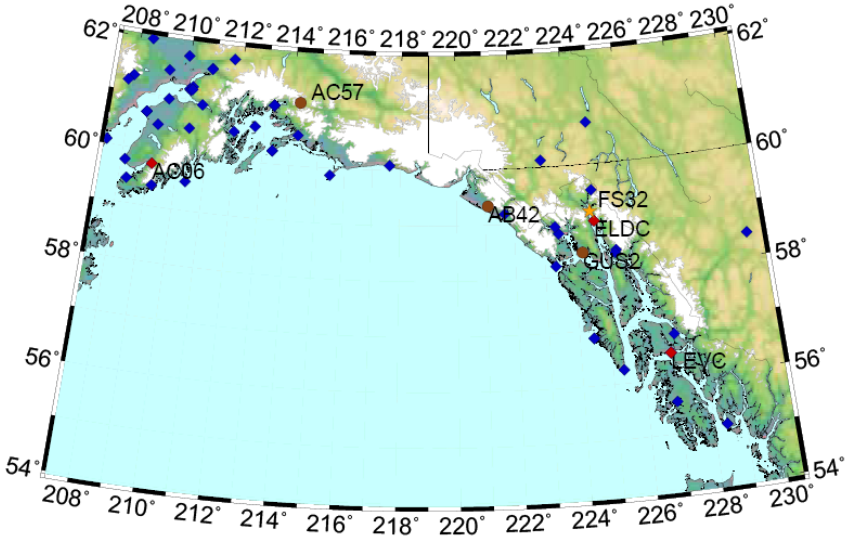

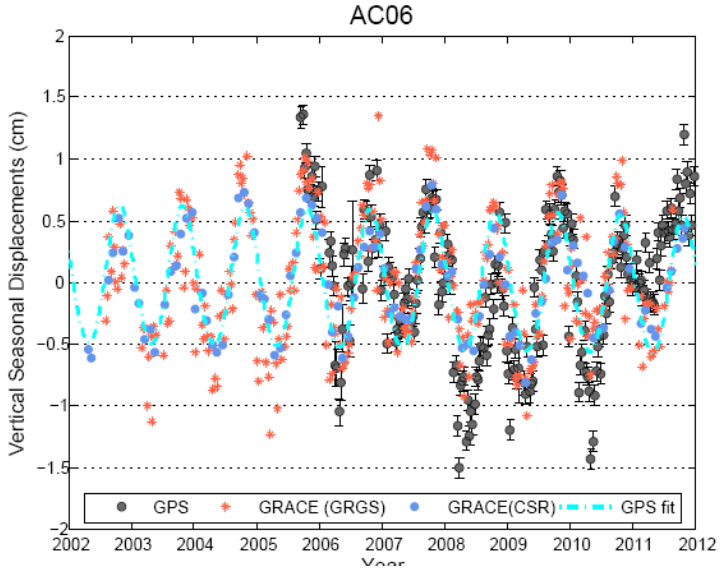

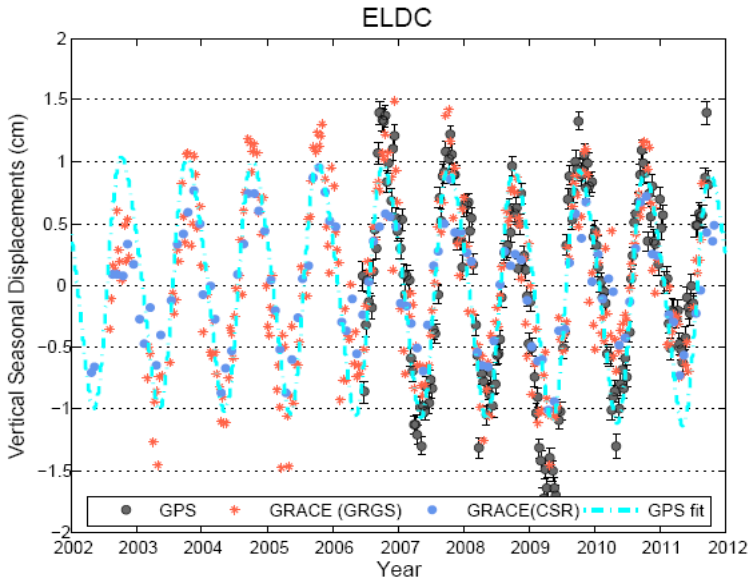

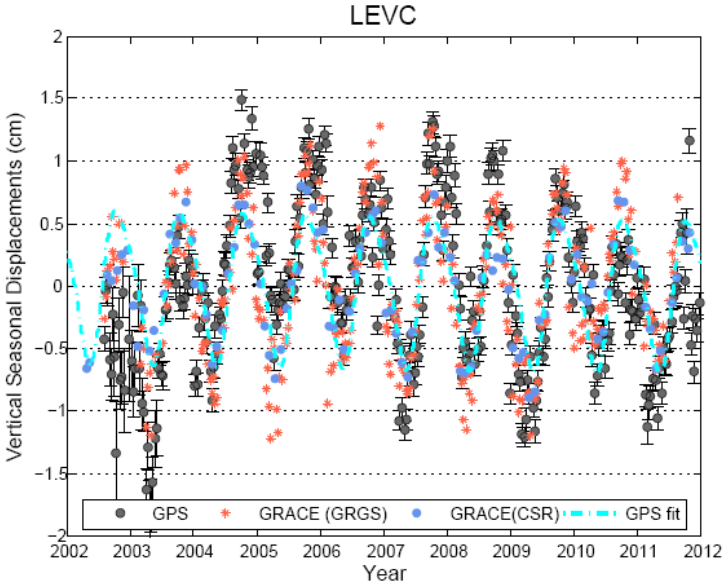

Southern Alaska: WRMS Reduction

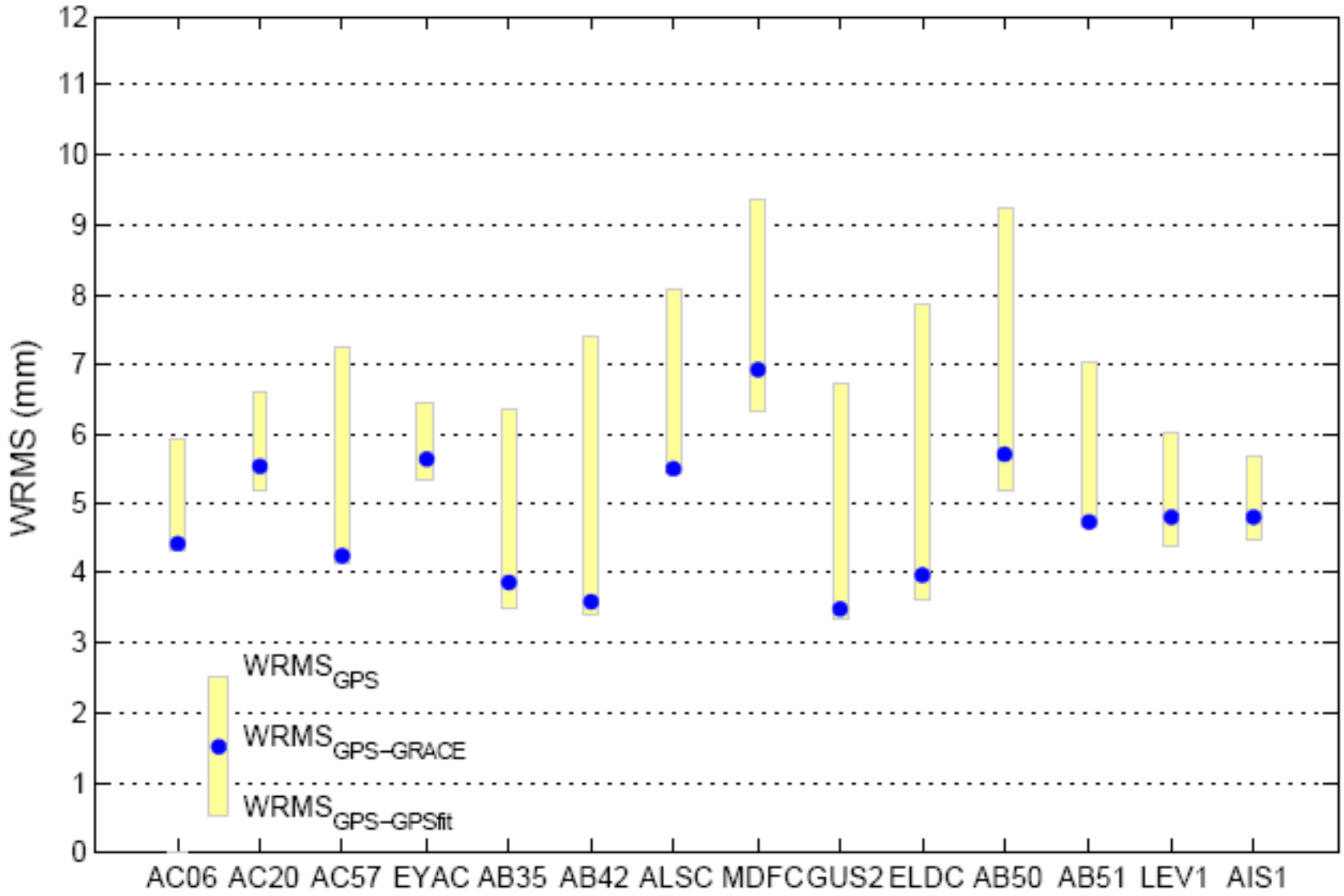

Southern Alaska: WRMS Reduction Ratio

$$Ratio_{WRMS\_reduction} = \frac{WRMS_{GPS} - WRMS_{GPS-GRACE}}{WRMS_{GPS} - WRMS_{GPS-GPS_{fit}}}$$

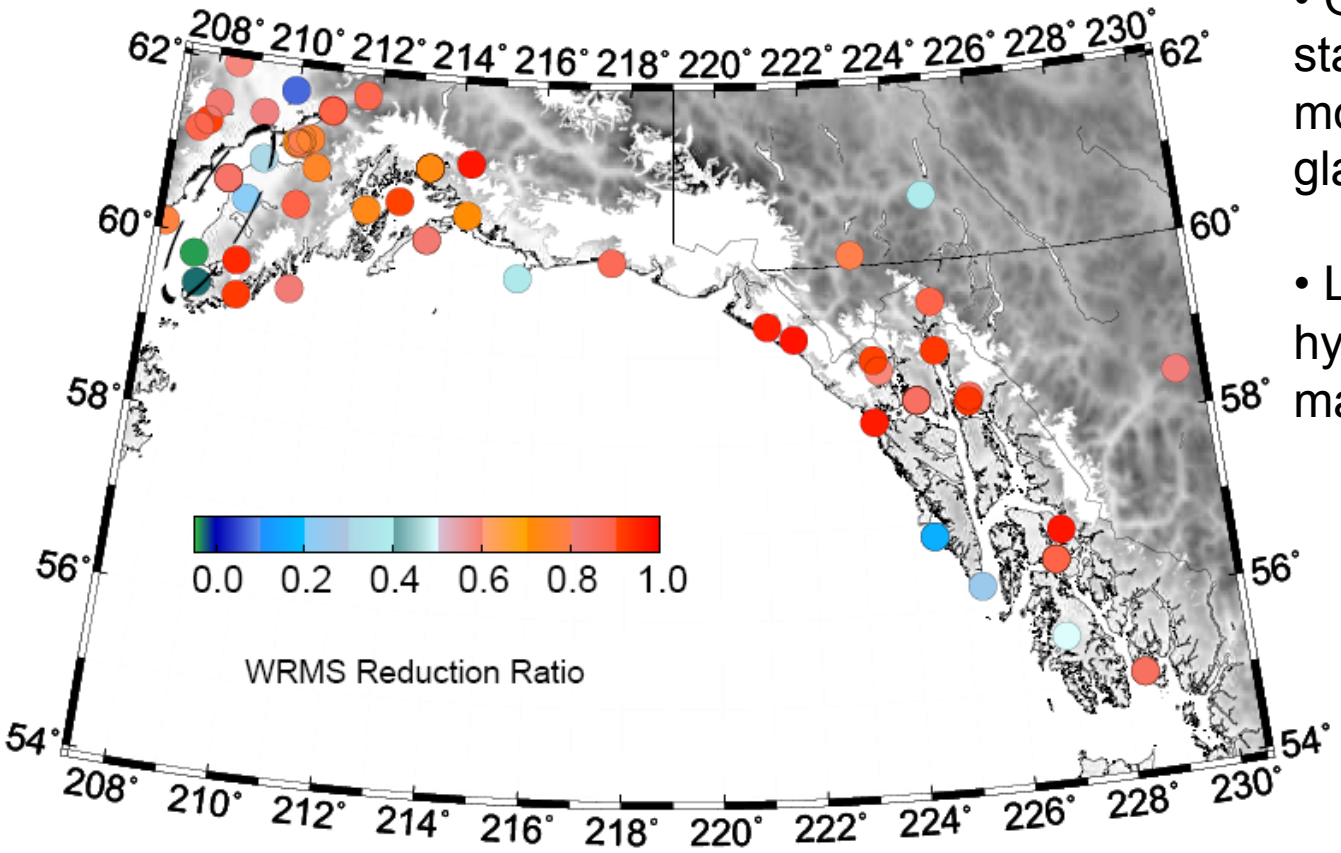

- Good correlation for stations close to high mountains and heavily glaciated areas.
- Long-wavelength hydrological seasonal mass loading dominates.

Southern Alaska: Seasonal Effect on Campaign GPS Measurements

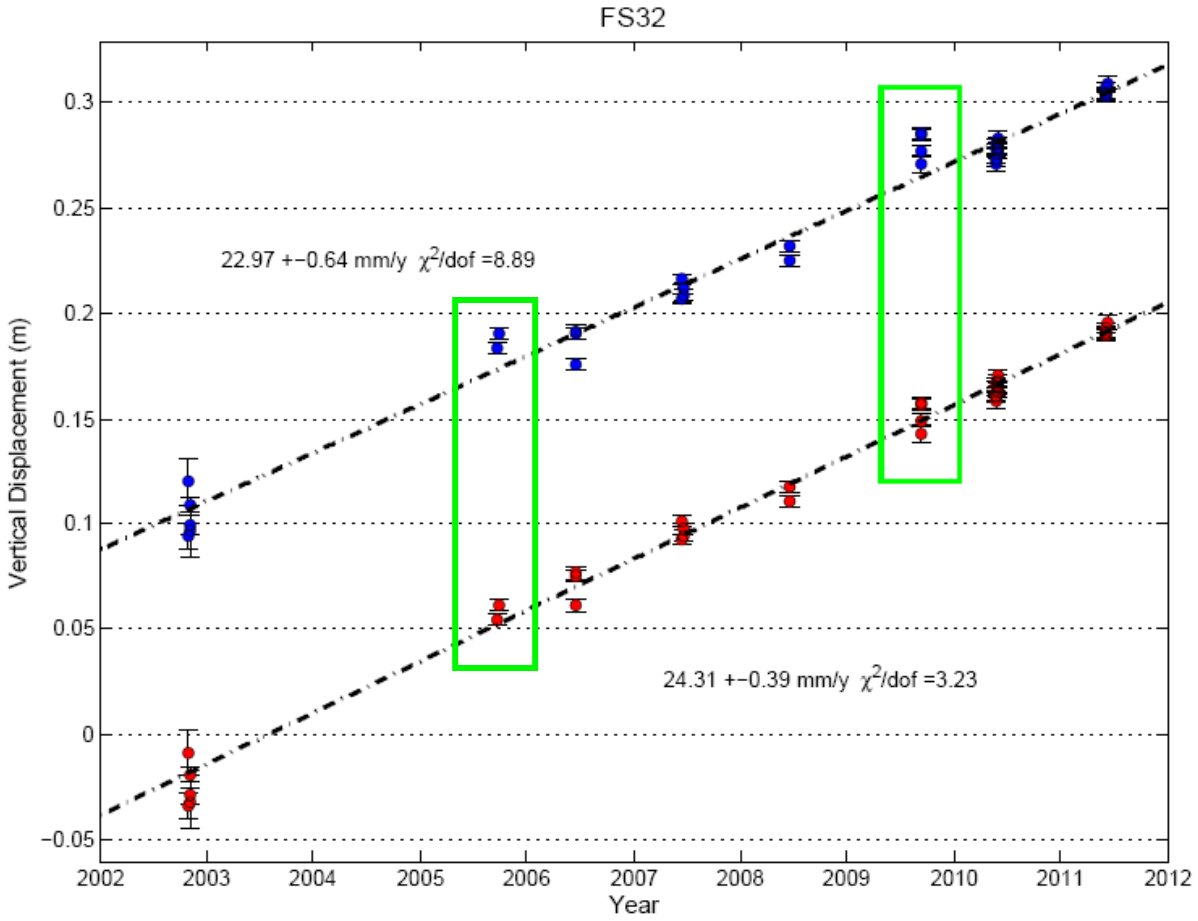

FS32: located near Juneau Ice Field.

Comparison: Nepal Himalaya and Southern Alaska

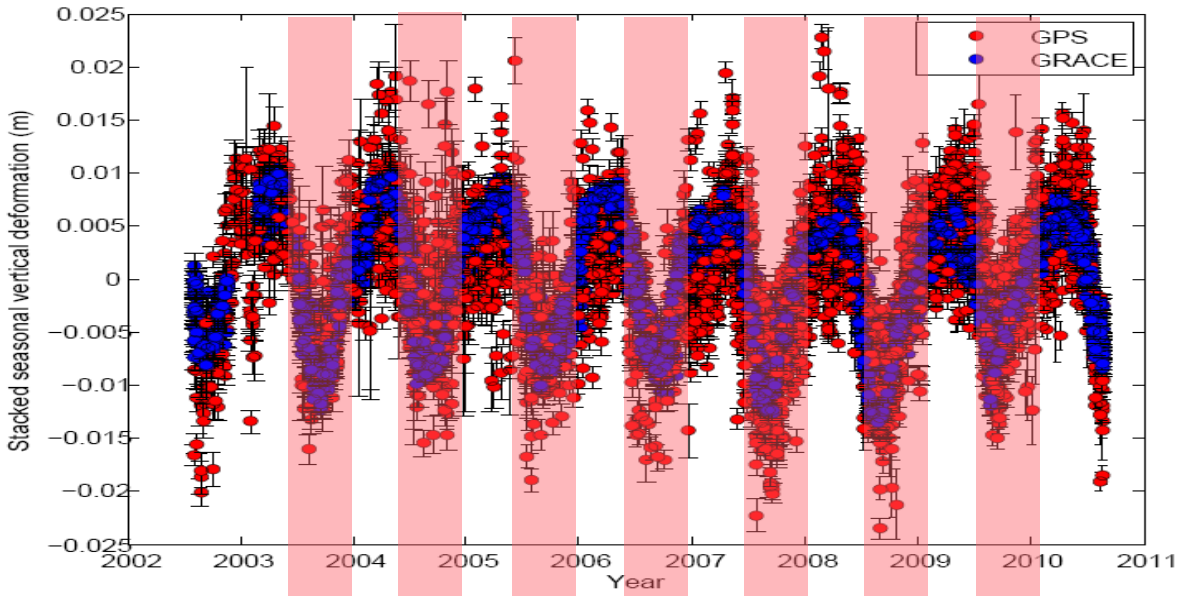

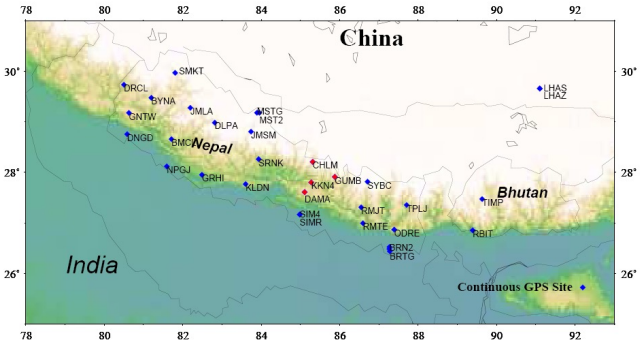

Main Source: **Monsoon in the summer.**

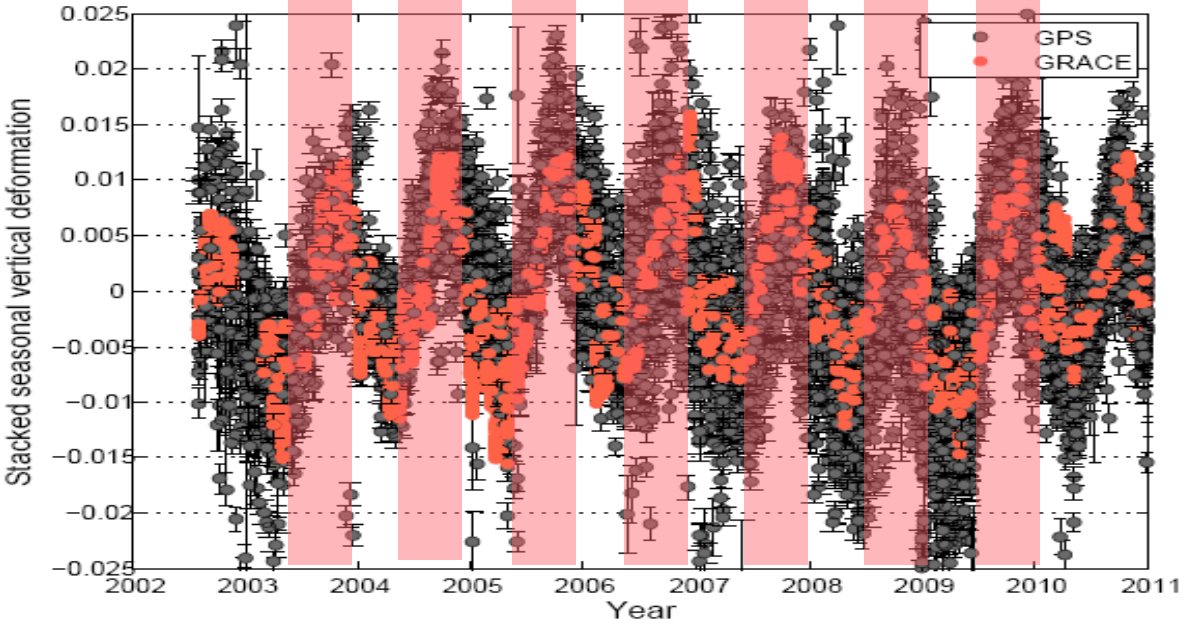

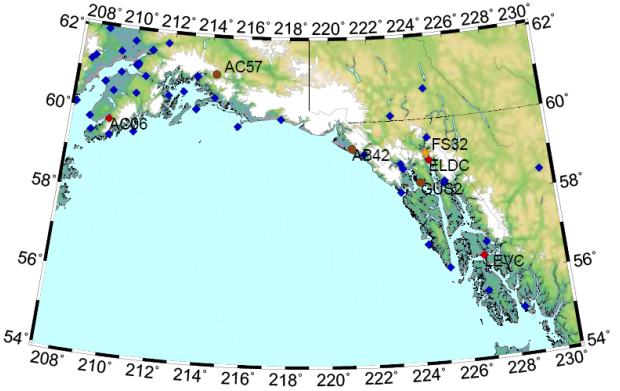

Comparison: Nepal Himalaya and Southern Alaska

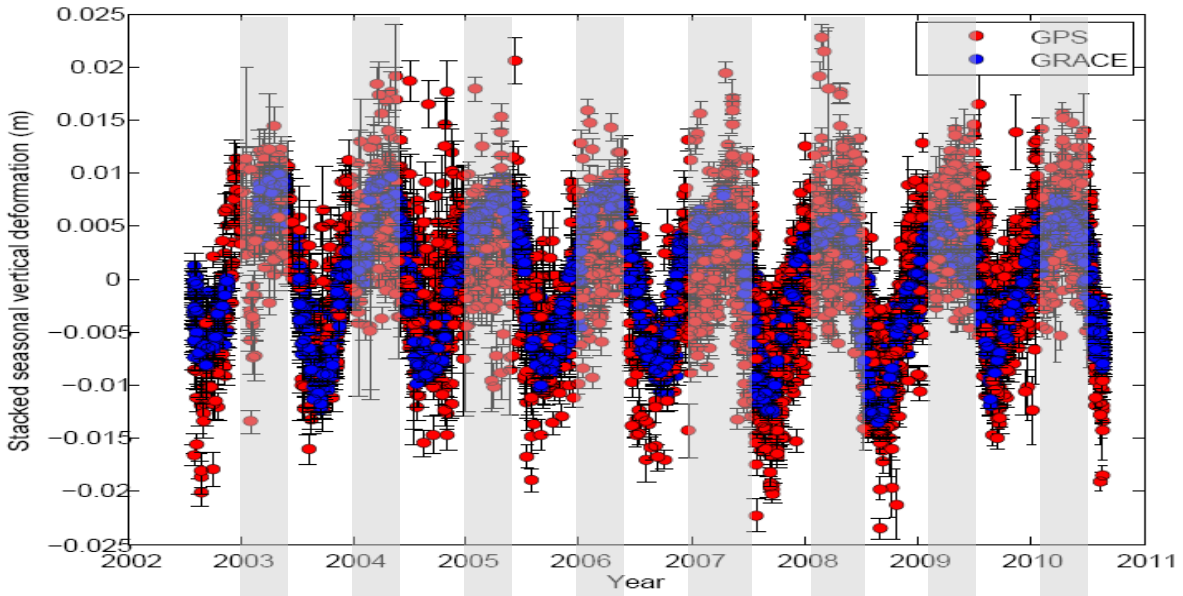

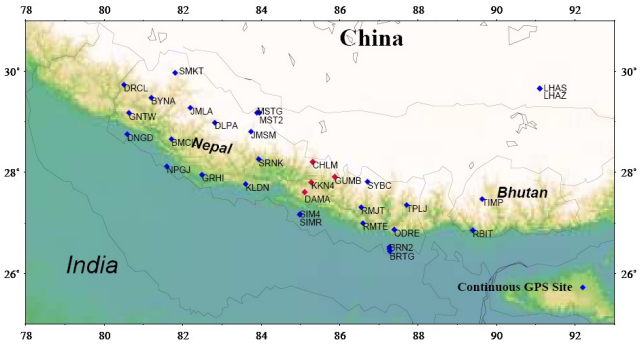

Main Source: **Monsoon in the summer.**

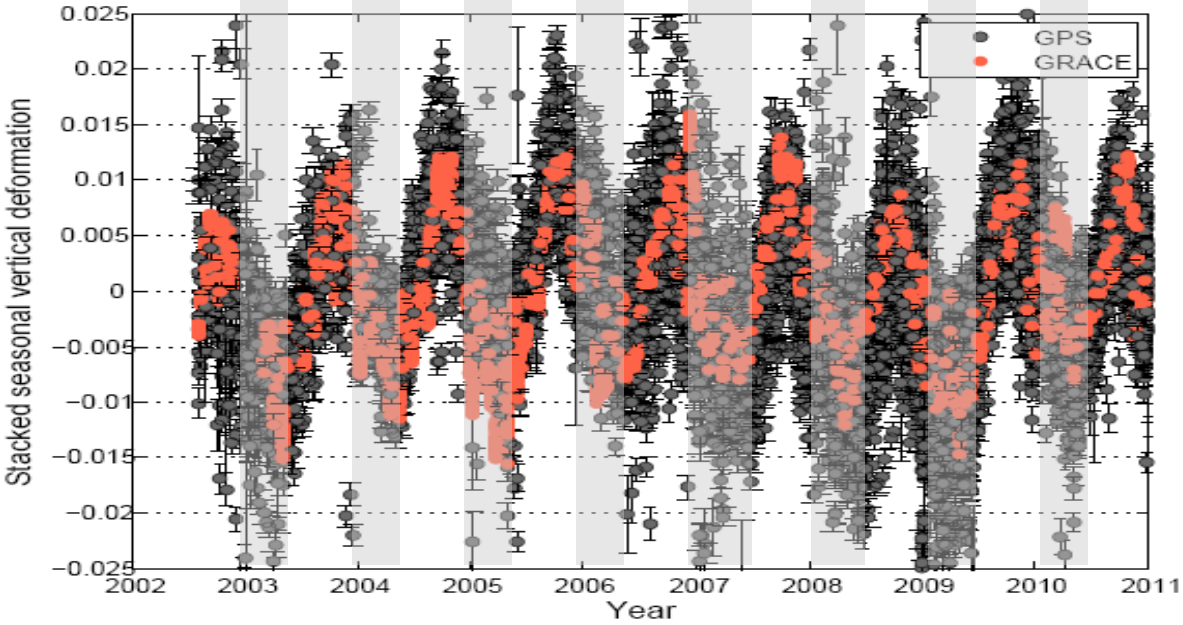

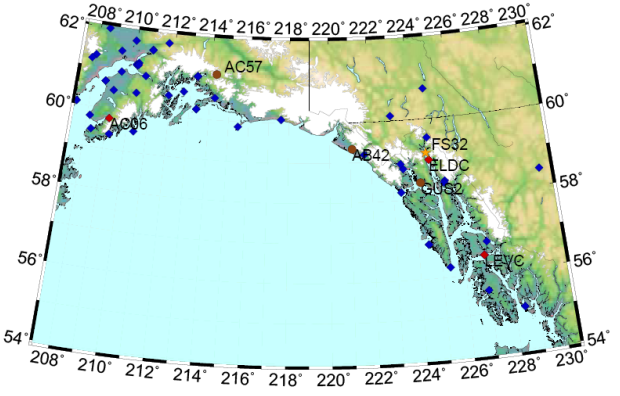

Main Source: **Snow in the winter.**

Continuous GPS Measurements

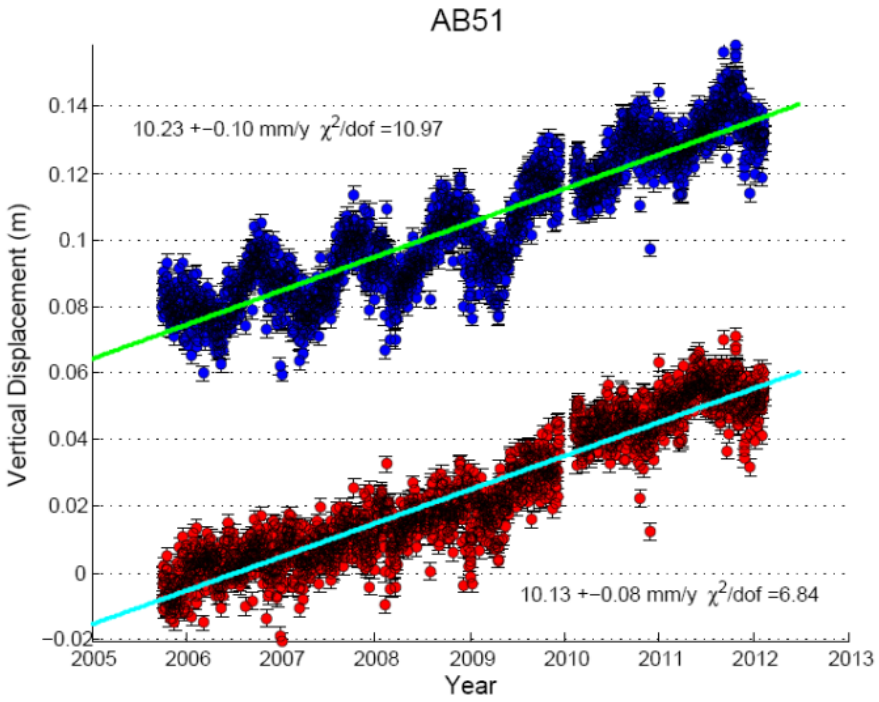

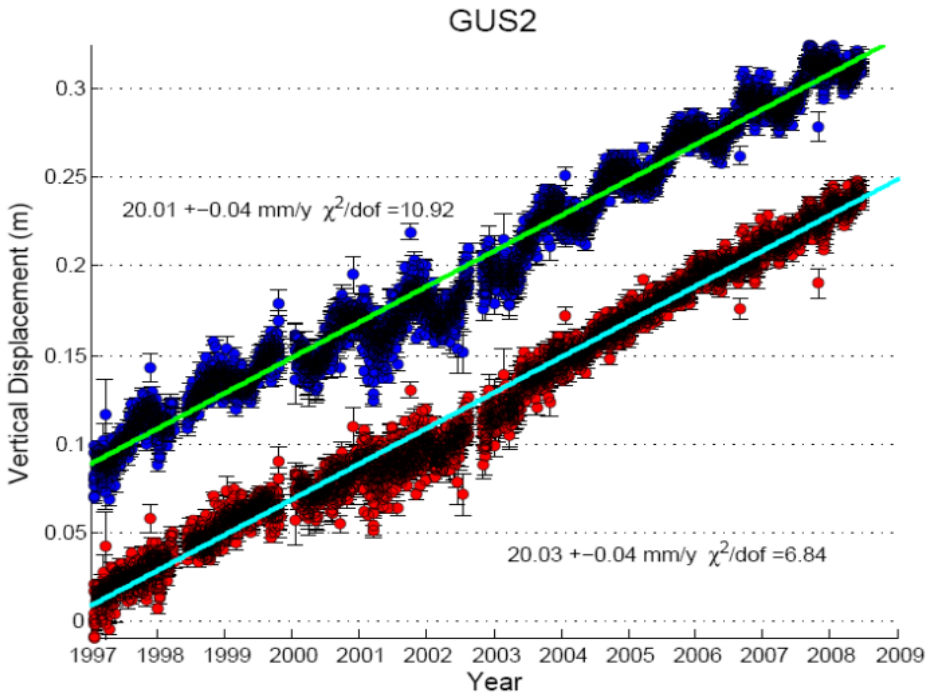

Application: Slow Slip Detection in Alaska

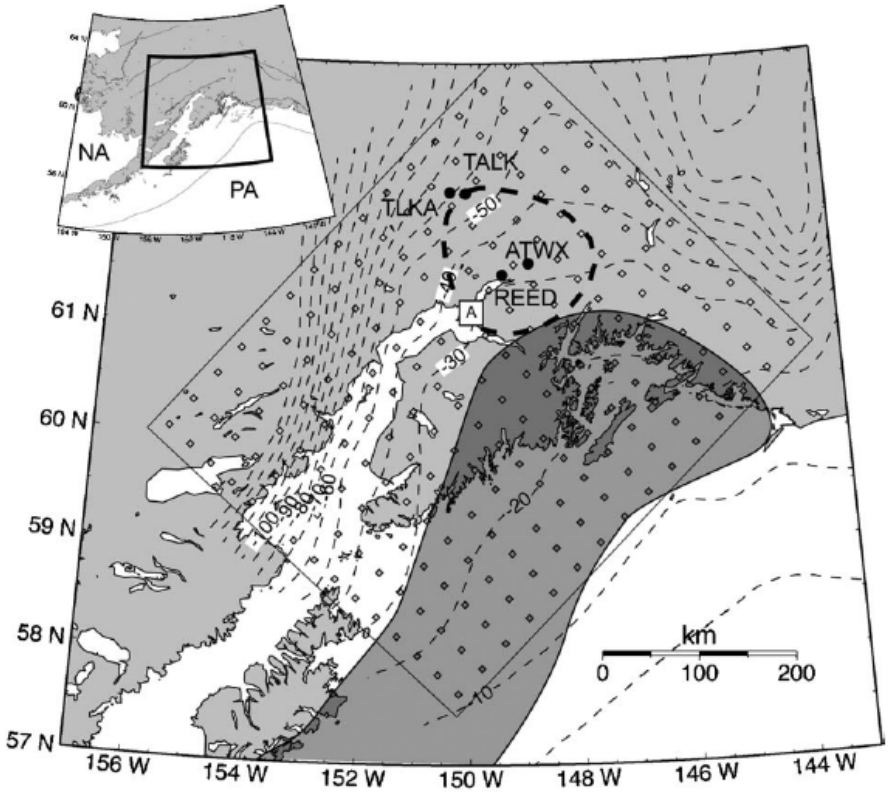

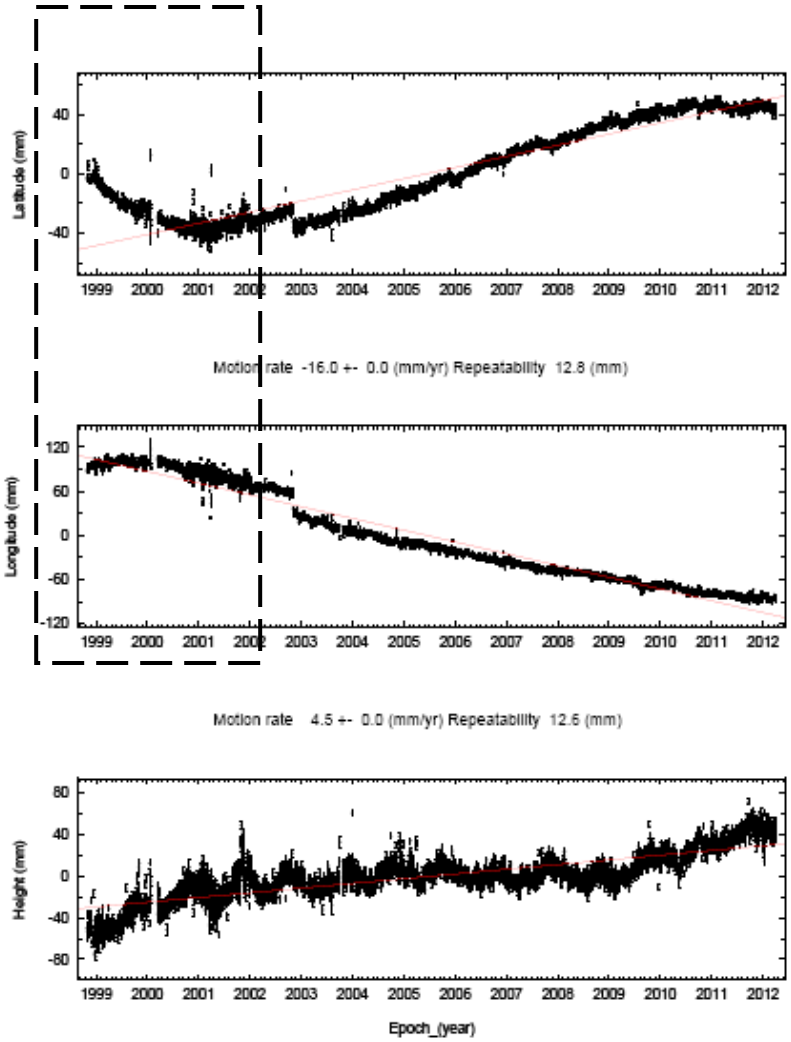

Ohta et al., 2006

Two Slow Slip Detected in Alaska

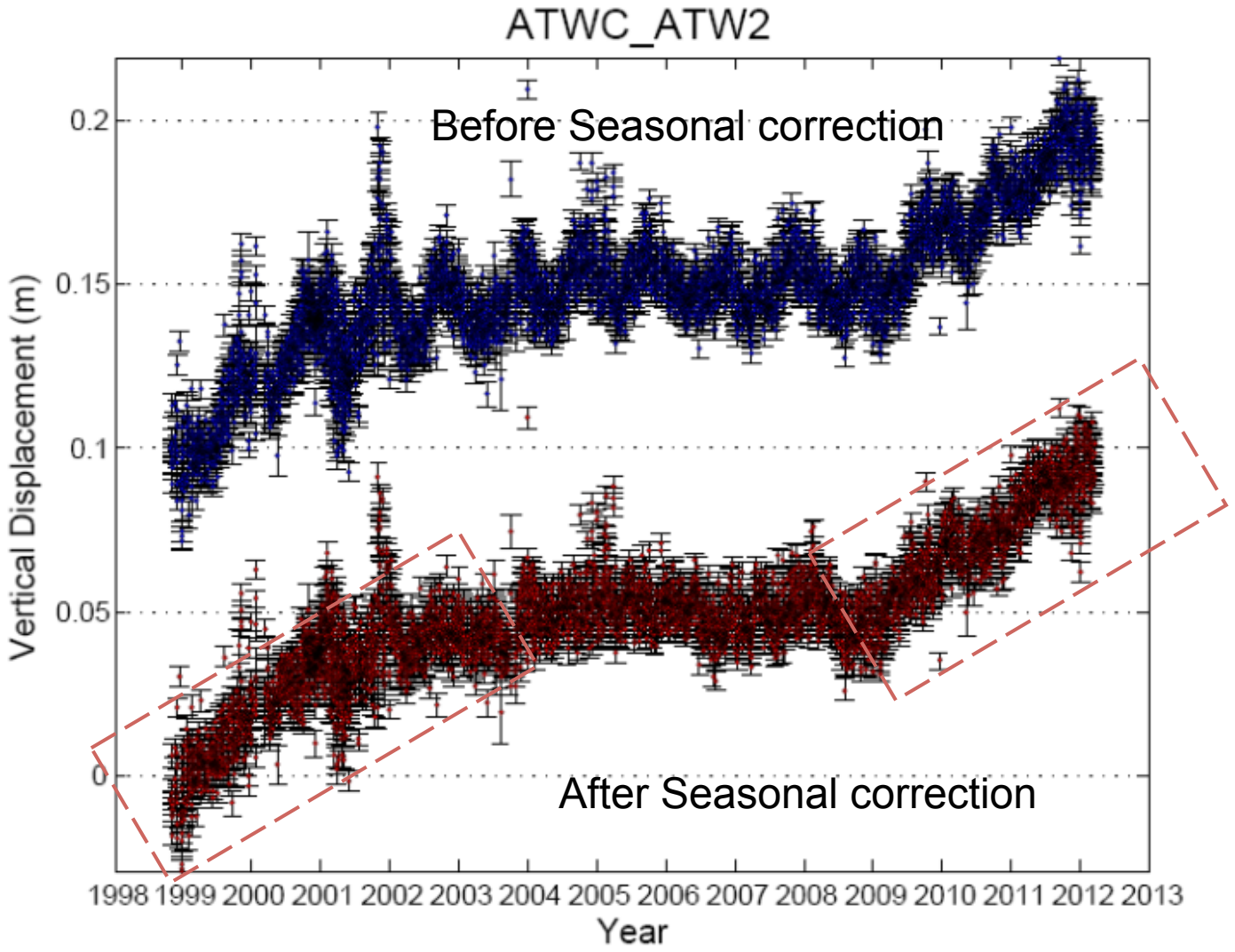

Water Loading
Rio Amazonas

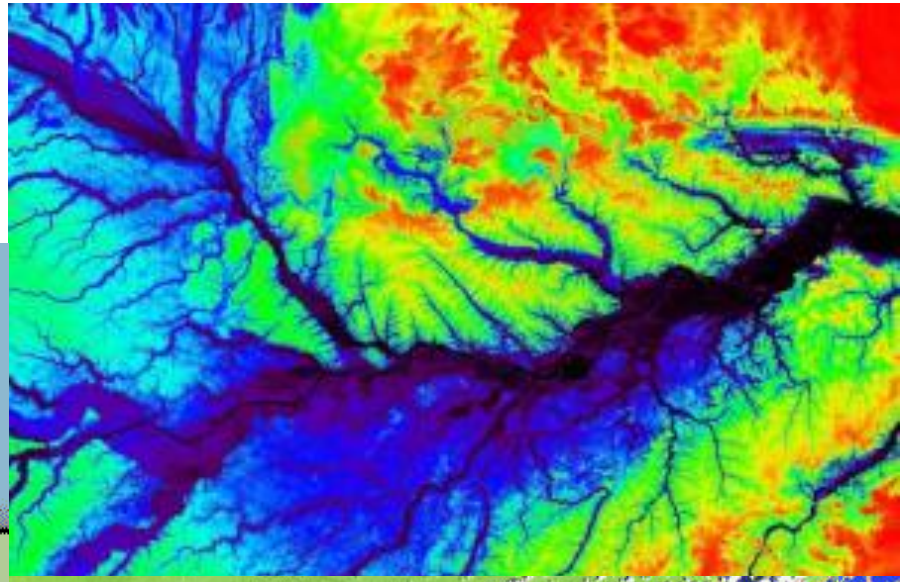

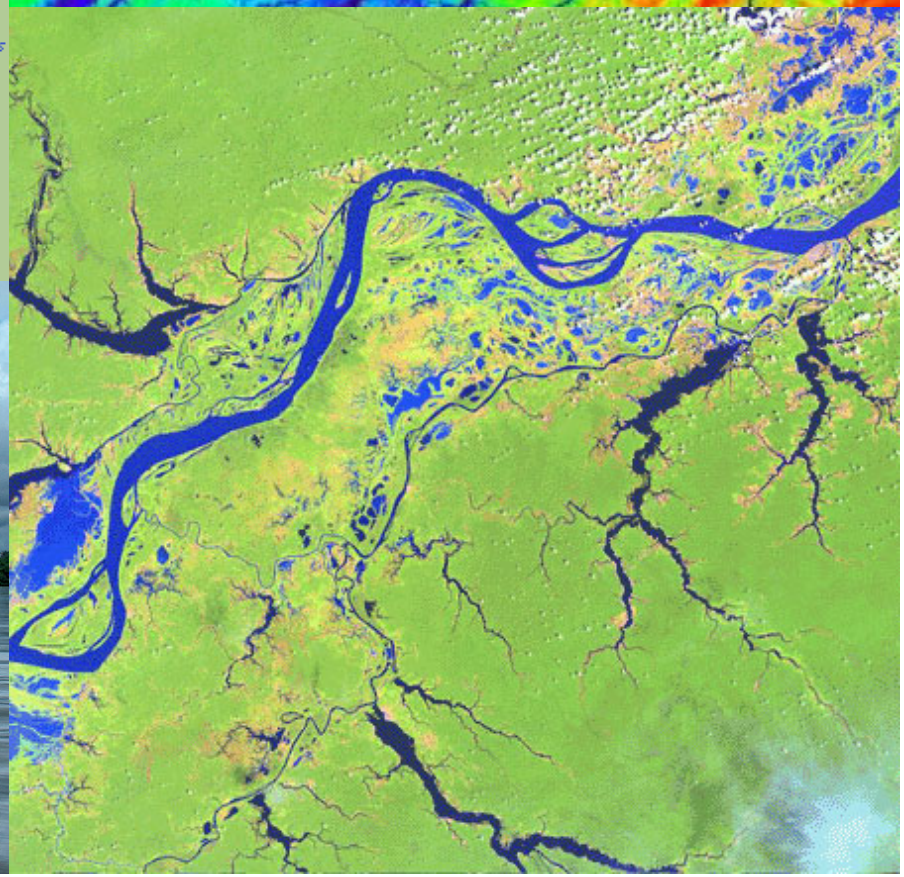

River Loading in the Amazon

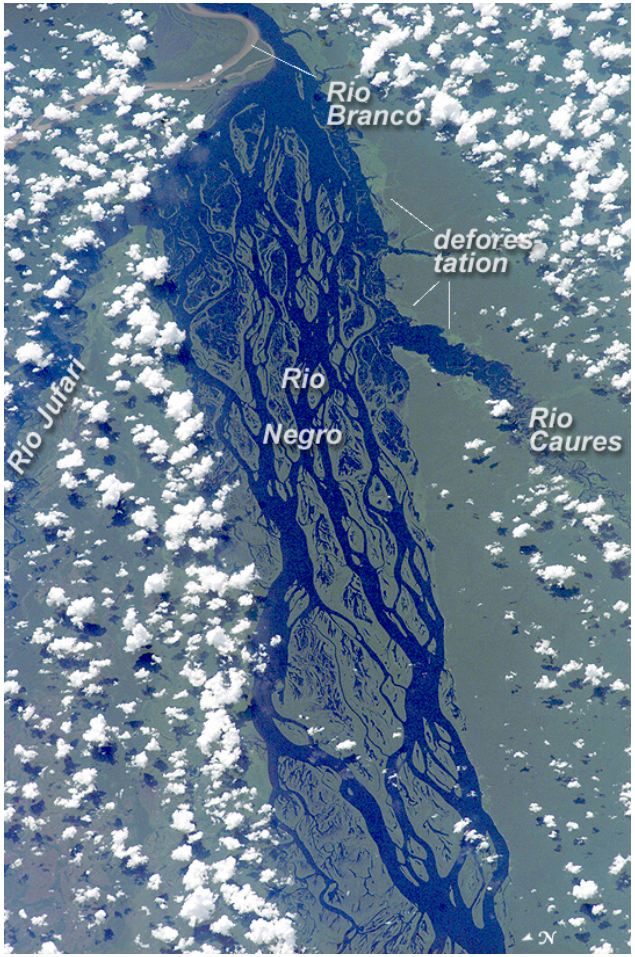

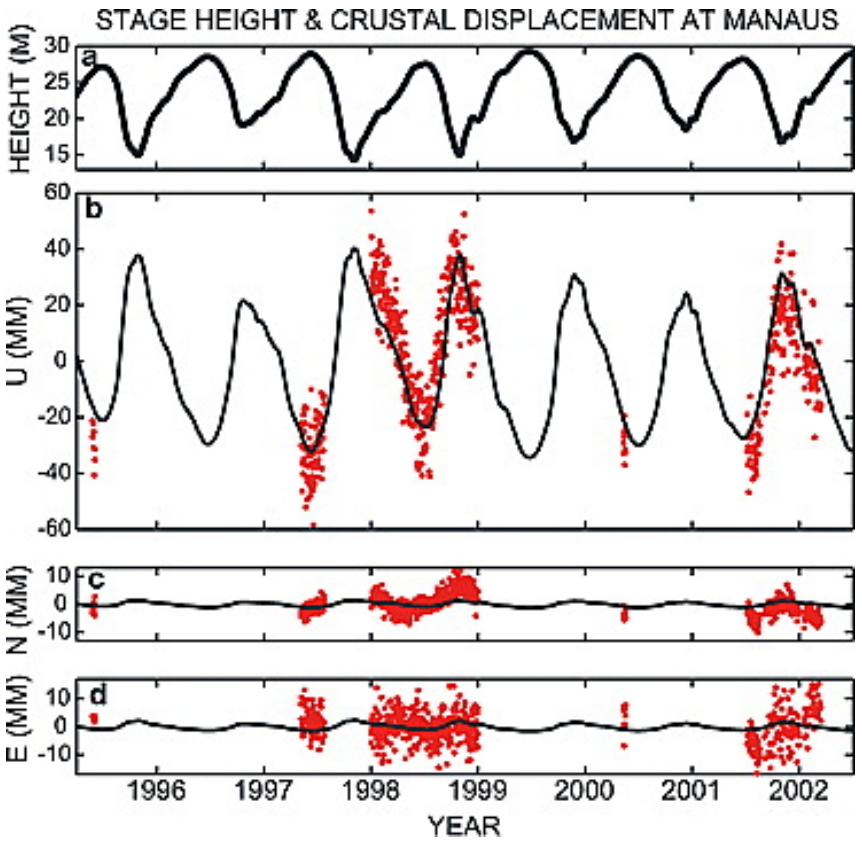

Bevis et al. (2005, GRL)

Detected in InSAR as well as GPS

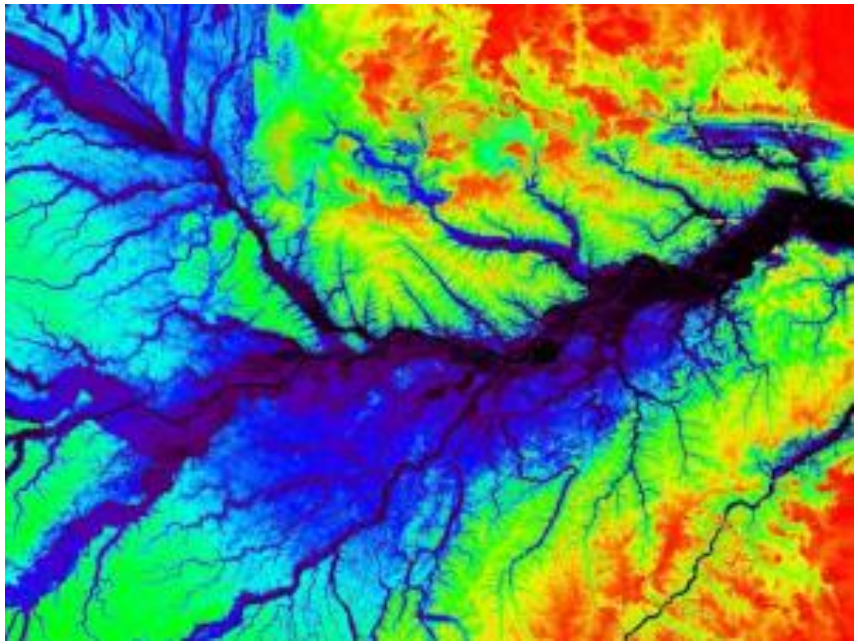

- Signal is about 8 cm peak to peak
- Perfectly anti-correlated with river stage level (zero time lag)
- Water load can be detected in InSAR data as well (blue depression at left).

Hydrologic Loading Models

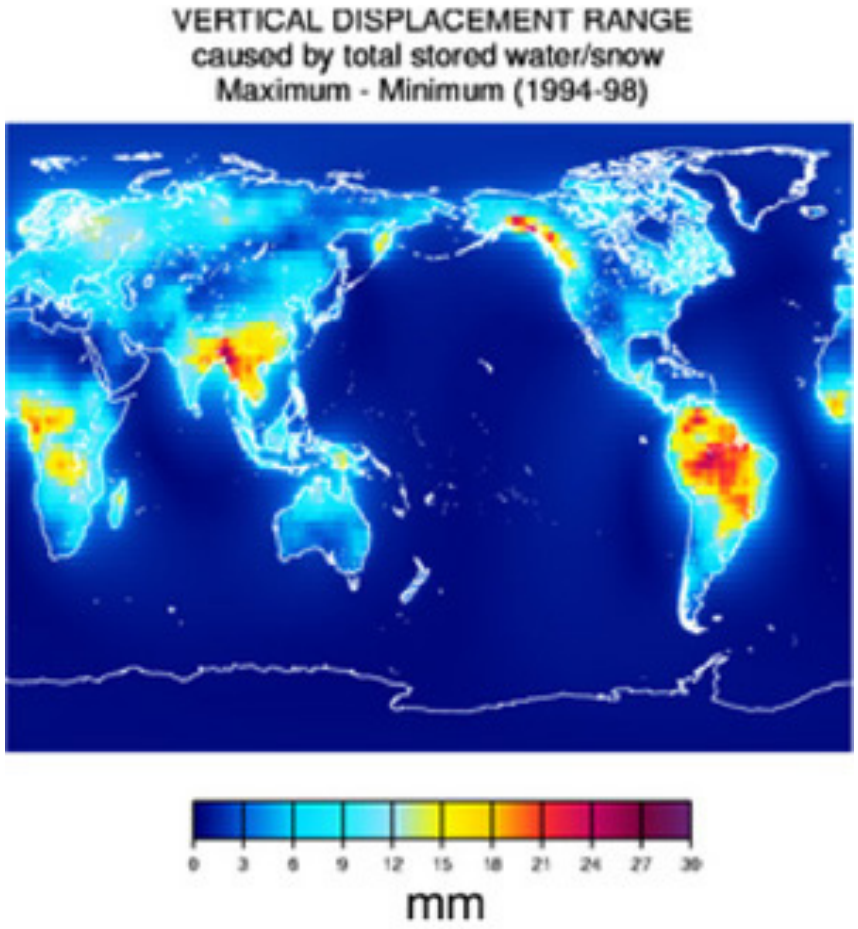

- Hydrologic models predict substantial seasonal variations
  - Largest amplitudes are tropical rain forest basins
    - Amazon
    - Congo
    - Mekong
  - And SE Alaska!
- Caused by local accumulation + transport of water.

Hydrologic Loading Models

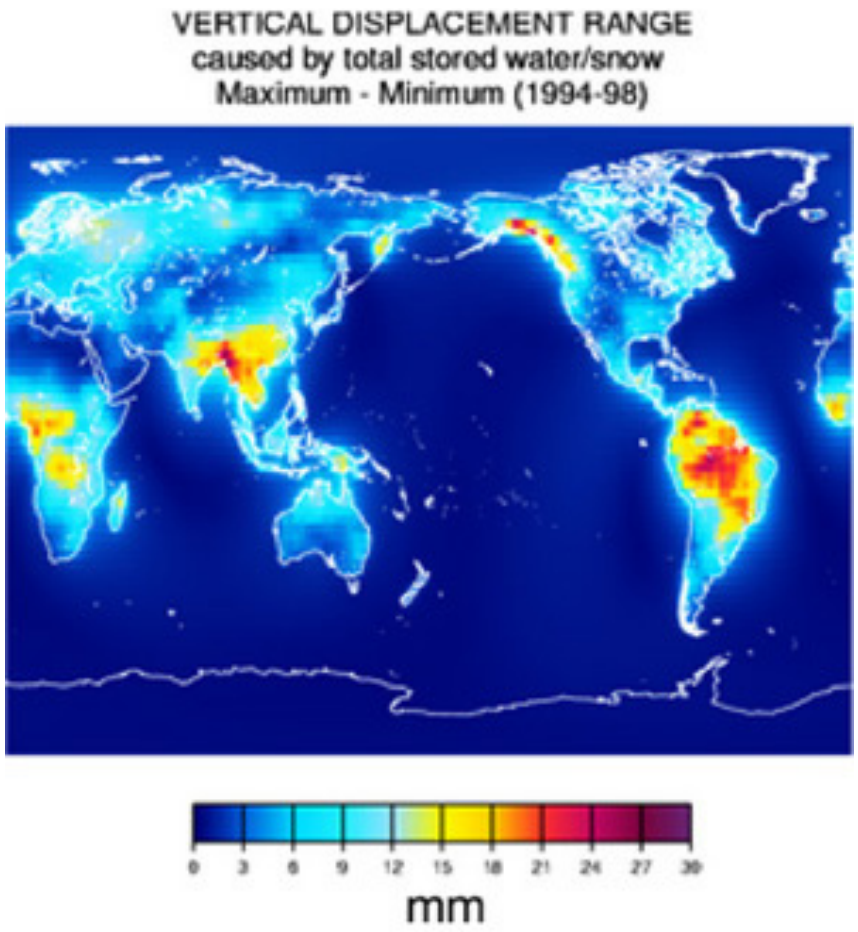

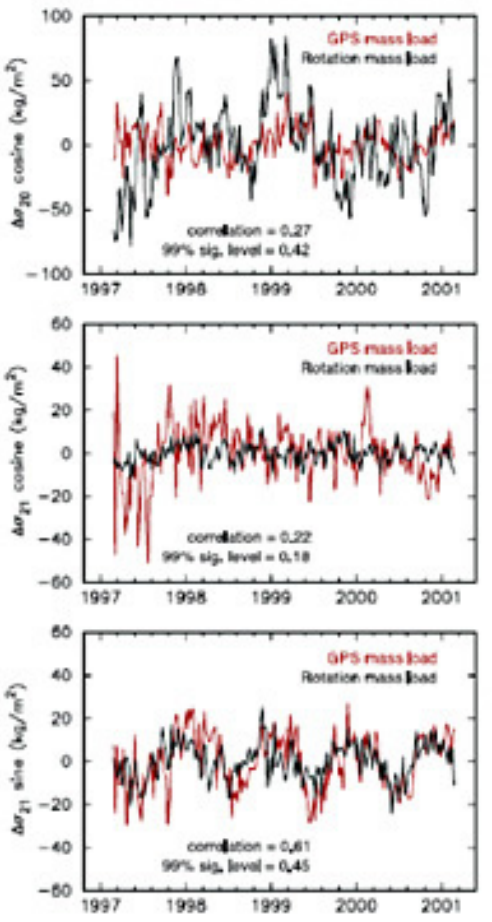

Van Dam et al. (2001)

West Coast Drought

GPS provides a new

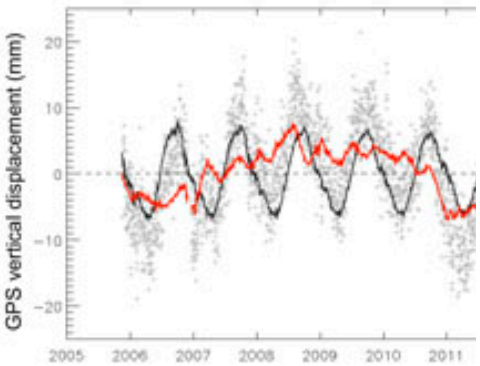

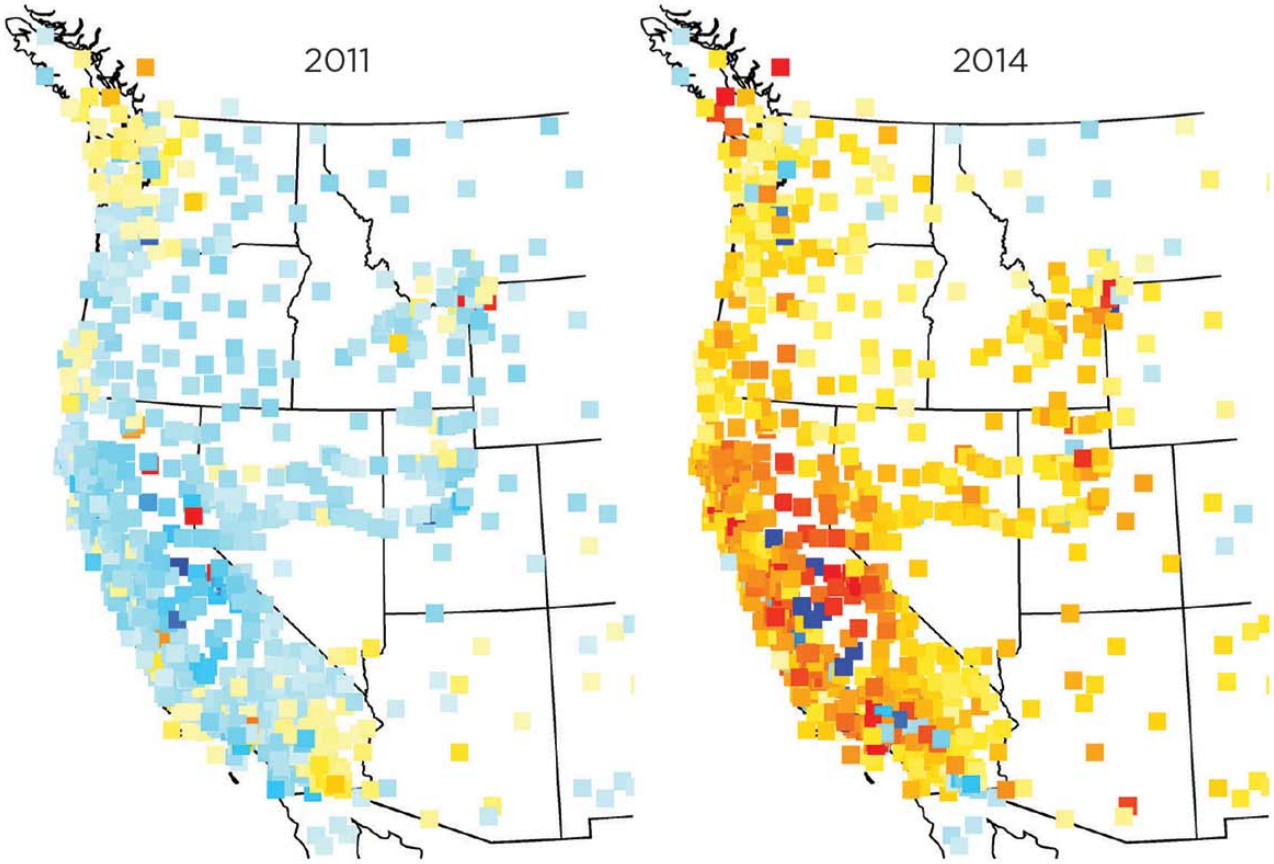

Maps of GPS points in the western U.S., with blue indicating a drop in land height and yellow-red reflecting a rise.

Vertical Displacement (mm)

-15 -10 -5 0 5 10 15

Borsa et al. (2014)

Comparison of Model to Data

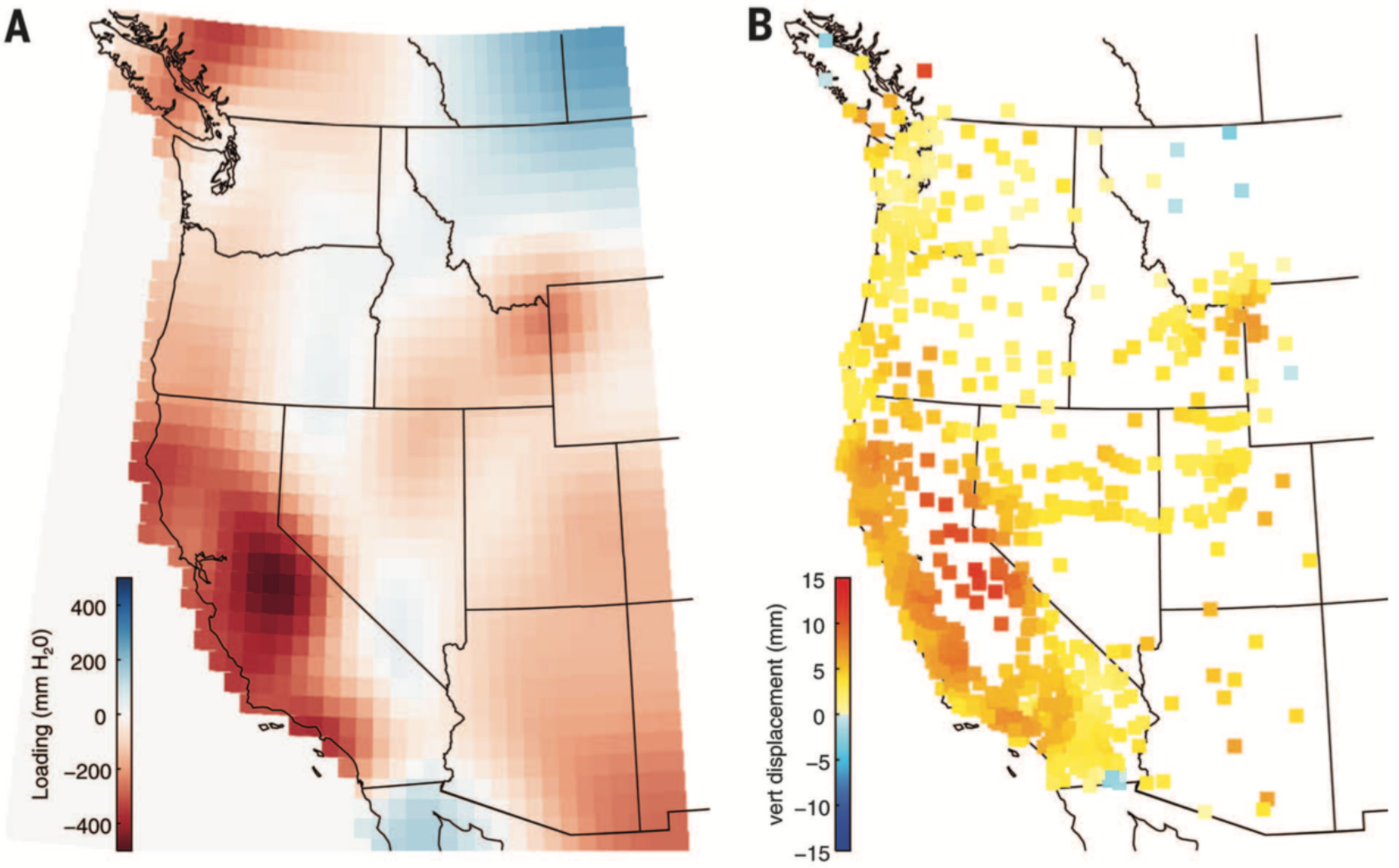

Borsa et al. (2014)

Western US Time Series Stacked

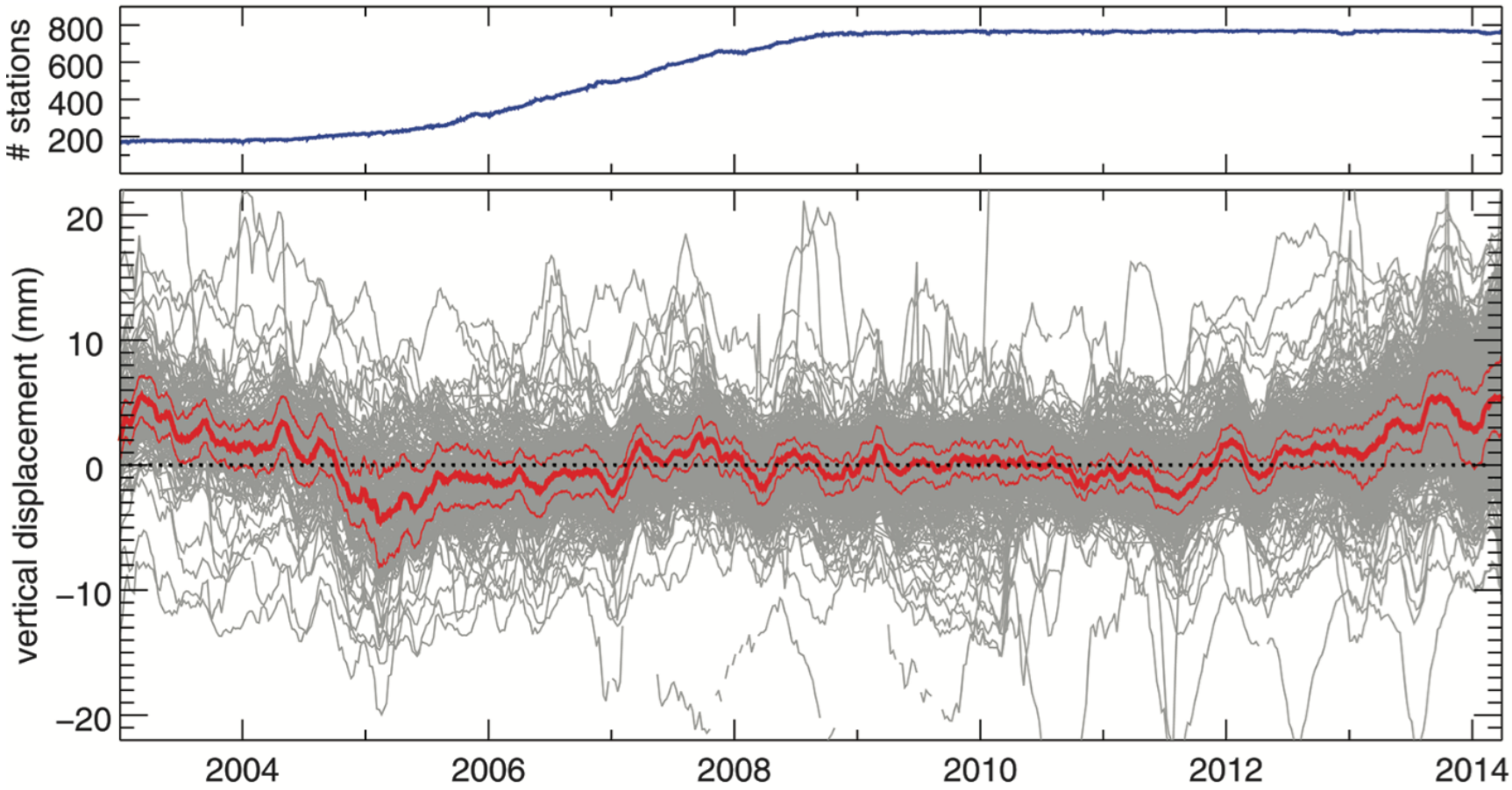

Borsa et al. (2014)

Progression of the Drought

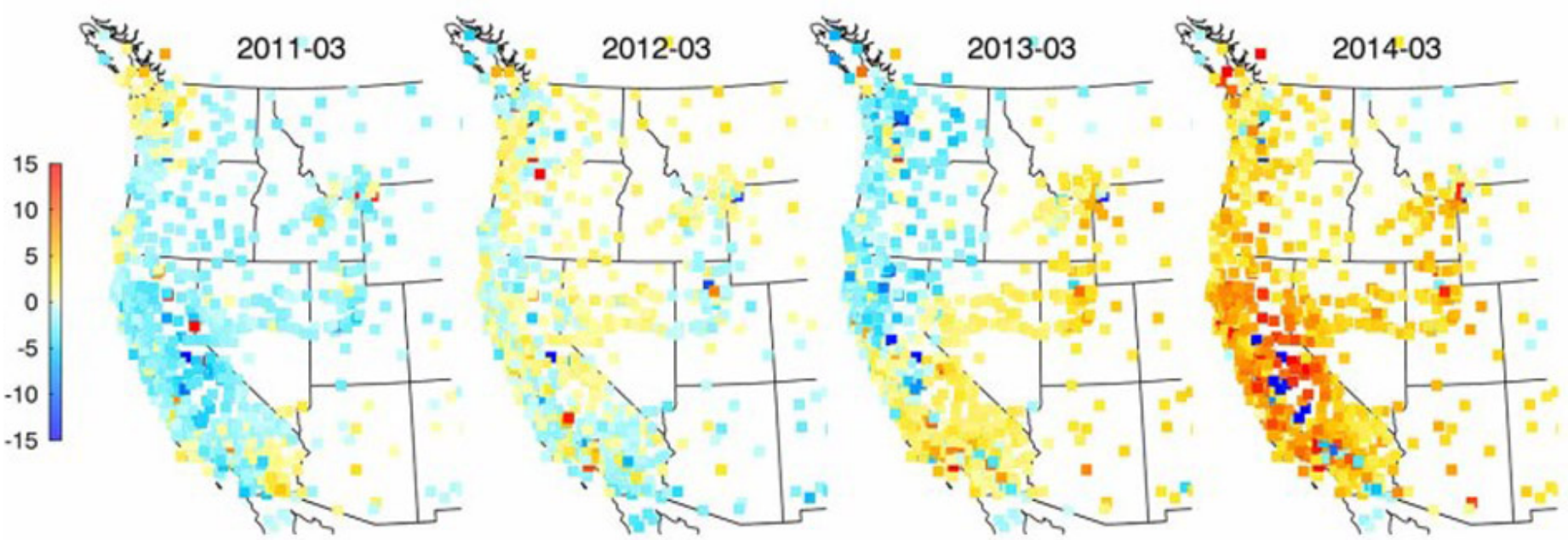

Borsa et al. (2014)

An animation of GRACE

- http://grace.jpl.nasa.gov/resources/5/

Global Scale Mass Transfer

- We expect there to be global seasonal mass transfer between hemispheres
  - Snow and ice accumulates at high latitudes during winter
  - But other factors might swamp that signal:
    - Asian monsoon (N Hemi. summer)
    - Tropical rainy seasons
- How to distinguish local variations from global variations hemispherical mass transfer?
  - Average over many sites!

Global Seasonal Mass Transfer

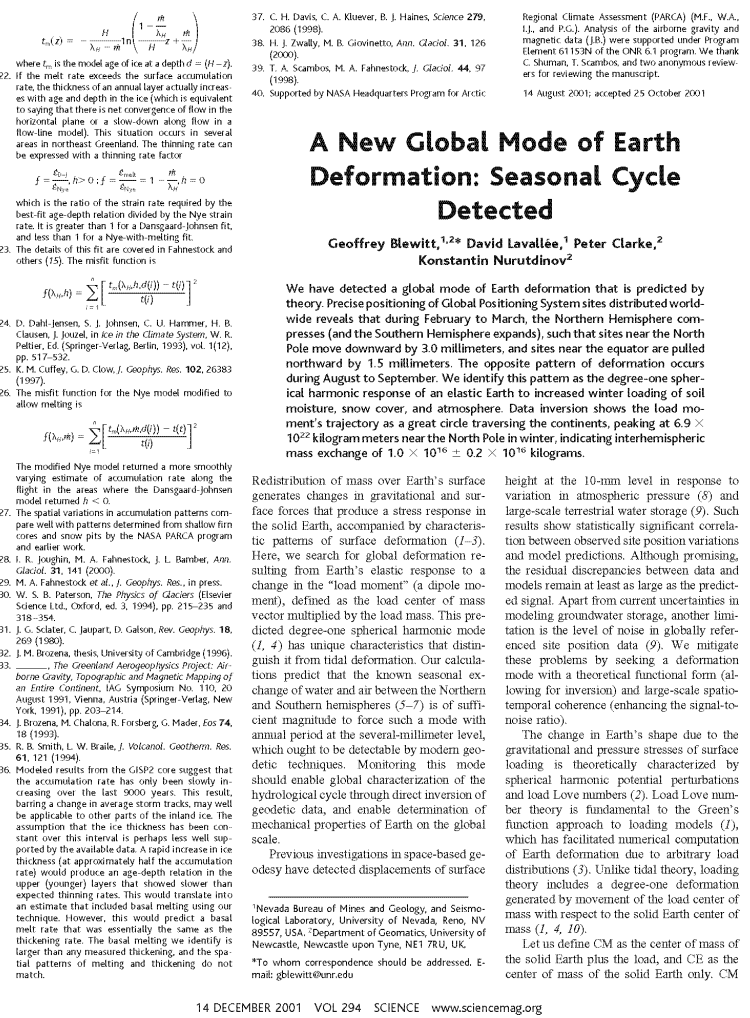

$$t_m(z) = -\frac{H}{\lambda_H - \dot{m}} \ln\left(\frac{1 - \frac{\dot{m}}{\lambda_H}}{\frac{H}{H-z} + \frac{\dot{m}}{\lambda_H}}\right)$$

where t_m is the model age of ice at a depth $d = (H - z)$.

22. If the melt rate exceeds the surface accumulation rate, the thickness of an annual layer actually increases with age and depth in the ice (which is equivalent to saying that there is net convergence of flow in the horizontal plane or a slow-down along flow in a flow-line model). This situation occurs in several areas in northeast Greenland. The thinning rate can be expressed with a thinning rate factor

$$f = \frac{\dot{\varepsilon}_{z=i}}{\dot{\varepsilon}_{z=s}}, h > 0\,; f = \frac{\dot{\varepsilon}_{z=b}}{\dot{\varepsilon}_{z=s}} = 1 - \frac{\dot{m}}{\lambda_H}, h = 0$$

which is the ratio of the strain rate required by the best-fit age-depth relation divided by the Nye strain rate. It is greater than 1 for a Dansgaard-Johnsen fit, and less than 1 for a Nye-with-melting fit.

23. The details of this fit are covered in Fahnestock and others (*15*). The misfit function is

$$f(\lambda_H, h) = \sum_{i=1}^{n}\left[\frac{t_m(\lambda_H, h, d(i)) - t(i)}{t(i)}\right]^2$$

24. D. Dahl-Jensen, S. J. Johnsen, C. U. Hammer, H. B. Clausen, J. Jouzel, in *Ice in the Climate System*, W. R. Peltier, Ed. (Springer-Verlag, Berlin, 1993), vol. 1(12), pp. 517–532.
25. K. M. Cuffey, G. D. Clow, *J. Geophys. Res.* **102**, 26383 (1997).
26. The misfit function for the Nye model modified to allow melting is

$$f(\lambda_H, \dot{m}) = \sum_{i=1}^{n}\left[\frac{t_m(\lambda_H, \dot{m}, d(i)) - t(i)}{t(i)}\right]^2$$

The modified Nye model returned a more smoothly varying estimate of accumulation rate along the flight in the areas where the Dansgaard-Johnsen model returned $h < 0$.

27. The spatial variations in accumulation patterns compare well with patterns determined from shallow firn cores and snow pits by the NASA PARCA program and earlier work.
28. I. R. Joughin, M. A. Fahnestock, J. L. Bamber, *Ann. Glaciol.* **31**, 141 (2000).
29. M. A. Fahnestock *et al.*, *J. Geophys. Res.*, in press.
30. W. S. B. Paterson, *The Physics of Glaciers* (Elsevier Science Ltd., Oxford, ed. 3, 1994), pp. 215–235 and 318–354.
31. J. G. Sclater, C. Jaupart, D. Galson, *Rev. Geophys.* **18**, 269 (1980).
32. J. M. Brozena, thesis, University of Cambridge (1996).
33. ———, *The Greenland Aerogeophysics Project: Airborne Gravity, Topographic and Magnetic Mapping of an Entire Continent*, IAG Symposium No. 110, 20 August 1991, Vienna, Austria (Springer-Verlag, New York, 1991), pp. 203–214.
34. J. Brozena, M. Chaloma, R. Forsberg, G. Mader, *Eos* **74**, 18 (1993).
35. R. B. Smith, L. W. Braile, *J. Volcanol. Geotherm. Res.* **61**, 121 (1994).
36. Modeled results from the GISP2 core suggest that the accumulation rate has only been slowly increasing over the last 9000 years. This result, barring a change in average storm tracks, may well be applicable to other parts of the inland ice. The assumption that the ice thickness has been constant over this interval is perhaps less well supported by the available data. A rapid increase in ice thickness (at approximately half the accumulation rate) would produce an age-depth relation in the upper (younger) layers that showed slower than expected thinning rates. This would translate into an estimate that included basal melting using our technique. However, this would predict a basal melt rate that was essentially the same as the thickening rate. The basal melting we identify is larger than any measured thickening, and the spatial patterns of melting and thickening do not match.

37. C. H. Davis, C. A. Kluever, B. J. Haines, *Science* **279**, 2086 (1998).
38. H. J. Zwally, M. B. Giovinetto, *Ann. Glaciol.* **31**, 126 (2000).
39. T. A. Scambos, M. A. Fahnestock, *J. Glaciol.* **44**, 97 (1998).
40. Supported by NASA Headquarters Program for Arctic Regional Climate Assessment (PARCA) (M.F., W.A., I.J., and P.G.). Analysis of the airborne gravity and magnetic data (J.B.) were supported under Program Element 61153N of the ONR 6.1 program. We thank C. Shuman, T. Scambos, and two anonymous reviewers for reviewing the manuscript.

14 August 2001; accepted 25 October 2001

A New Global Mode of Earth Deformation: Seasonal Cycle Detected

Geoffrey Blewitt,[1,2]* David Lavallée,[1] Peter Clarke,[2] Konstantin Nurutdinov[2]

We have detected a global mode of Earth deformation that is predicted by theory. Precise positioning of Global Positioning System sites distributed worldwide reveals that during February to March, the Northern Hemisphere compresses (and the Southern Hemisphere expands), such that sites near the North Pole move downward by 3.0 millimeters, and sites near the equator are pulled northward by 1.5 millimeters. The opposite pattern of deformation occurs during August to September. We identify this pattern as the degree-one spherical harmonic response of an elastic Earth to increased winter loading of soil moisture, snow cover, and atmosphere. Data inversion shows the load moment's trajectory as a great circle traversing the continents, peaking at 6.9×10^{22} kilogram meters near the North Pole in winter, indicating interhemispheric mass exchange of $1.0 \times 10^{16} \pm 0.2 \times 10^{16}$ kilograms.

Redistribution of mass over Earth's surface generates changes in gravitational and surface forces that produce a stress response in the solid Earth, accompanied by characteristic patterns of surface deformation (*1–3*). Here, we search for global deformation resulting from Earth's elastic response to a change in the "load moment" (a dipole moment), defined as the load center of mass vector multiplied by the load mass. This predicted degree-one spherical harmonic mode (*1, 4*) has unique characteristics that distinguish it from tidal deformation. Our calculations predict that the known seasonal exchange of water and air between the Northern and Southern hemispheres (*5–7*) is of sufficient magnitude to force such a mode with annual period at the several-millimeter level, which ought to be detectable by modern geodetic techniques. Monitoring this mode should enable global characterization of the hydrological cycle through direct inversion of geodetic data, and enable determination of mechanical properties of Earth on the global scale.

Previous investigations in space-based geodesy have detected displacements of surface height at the 10-mm level in response to variation in atmospheric pressure (*8*) and large-scale terrestrial water storage (*9*). Such results show statistically significant correlation between observed site position variations and model predictions. Although promising, the residual discrepancies between data and models remain at least as large as the predicted signal. Apart from current uncertainties in modeling groundwater storage, another limitation is the level of noise in globally referenced site position data (*9*). We mitigate these problems by seeking a deformation mode with a theoretical functional form (allowing for inversion) and large-scale spatio-temporal coherence (enhancing the signal-to-noise ratio).

The change in Earth's shape due to the gravitational and pressure stresses of surface loading is theoretically characterized by spherical harmonic potential perturbations and load Love numbers (*2*). Load Love number theory is fundamental to the Green's function approach to loading models (*1*), which has facilitated numerical computation of Earth deformation due to arbitrary load distributions (*3*). Unlike tidal theory, loading theory includes a degree-one deformation generated by movement of the load center of mass with respect to the solid Earth center of mass (*1, 4, 10*).

Let us define CM as the center of mass of the solid Earth plus the load, and CE as the center of mass of the solid Earth only. CM

[1]Nevada Bureau of Mines and Geology, and Seismological Laboratory, University of Nevada, Reno, NV 89557, USA. [2]Department of Geomatics, University of Newcastle, Newcastle upon Tyne, NE1 7RU, UK.

*To whom correspondence should be addressed. E-mail: gblewitt@unr.edu

- Blewitt et al. (2001)
  - During February to March, the Northern Hemisphere compresses (and the Southern Hemisphere expands), such that sites near the North Pole move downward by 3.0 millimeters, and sites near the equator are pulled northward by 1.5 millimeters. The opposite pattern of deformation occurs during August to September. We identify this pattern as the degree-one spherical harmonic response of an elastic Earth to increased winter loading of soil moisture, snow cover, and atmosphere.

Results for Load Moment Vector

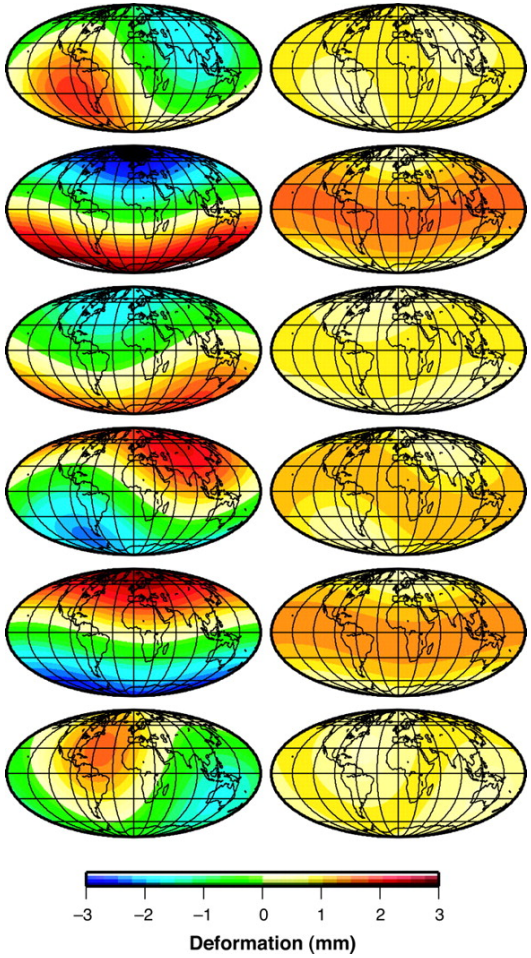

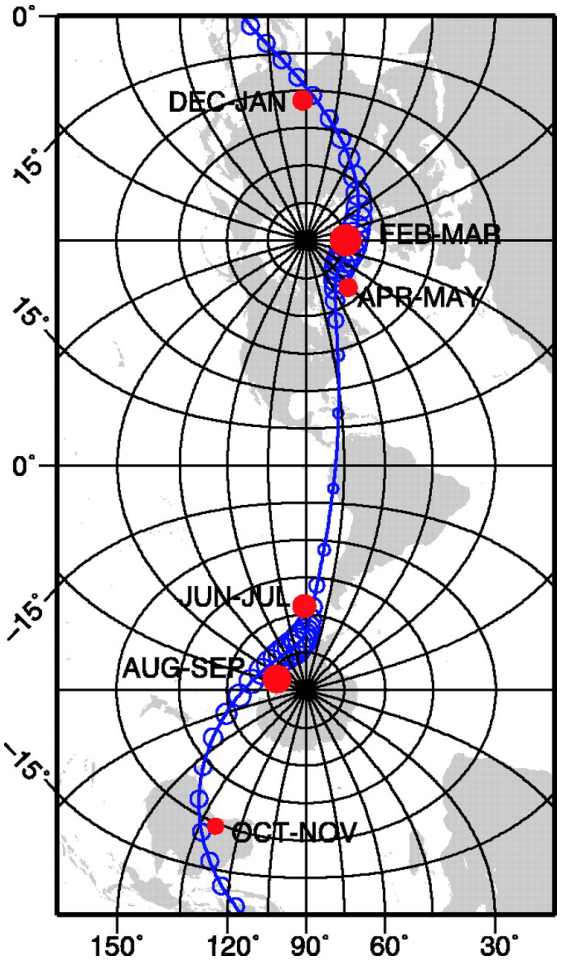

How Can You Detect This?

- Redistribution of mass over Earth's surface generates changes in gravitational and surface forces that produce a stress response in the solid Earth, accompanied by characteristic patterns of surface deformation
- First-order pattern is spherical harmonic degree 1
  - Degree 1 loads can be described by a "load moment" vector.

Definitions

- Load distributed in thin shell around earth
- CM is center of mass of solid earth + load
- CE is center of mass of solid earth only
- Offset of CE with respect to CM is:

$$\Delta \mathbf{r}_{\mathrm{CE}} = -M_{\mathrm{L}} \Delta \bar{\mathbf{r}}_{\mathrm{L}} / M_{\oplus} = -\mathbf{m}/M_{\oplus}$$

- This results in a deforming potential V_1

$$V_1(\phi, \lambda) = -g\hat{\mathrm{h}}.\Delta \mathbf{r}_{\mathrm{CE}} = g\hat{\mathrm{h}}.\mathbf{m}/M_{\oplus}$$

  – Where h is a unit vector pointing upward

Displacements in CE frame

- Displacements can be calculated easily for this deforming load potential. In the CE frame:

$$\Delta\bar{s}_h = h_1' V_1/g = h_1' \hat{\mathrm{h}}.\mathrm{m}/M_\oplus$$

$$\Delta\bar{s}_l = l_1' \hat{\mathrm{l}}.\nabla V_1/g = l_1' \hat{\mathrm{l}}.\mathrm{m}/M_\oplus$$

- Load Love numbers in CE frame are:
  - h_1' = -0.290; l_1' = 0.113
  - Meaning of the signs:
    - Positive load causes subsidence, h < 0
    - Positive load causes inward displacement, l > 0
  - Displacement proportional to ***load moment vector***

Peculiarities

- Sphere deforms to Sphere
  - This mode of deformation is unique, in that it compresses the hemisphere centered on the load moment, and expands the opposite hemisphere, such that a perfect sphere deforms to another perfect (but strained) sphere of identical diameter.
  - That is, the deformation is like a translation, although no two points actually move the same way.
- Equivalent to a seasonal geocenter variation

Applying the Theory

- GPS frame is not in CE or CM
  - Approximately CF = Center of Figure
    - Defined by the shape/position of the surface of Earth
- Transform equations to CF frame
  - Subtract the average displacement $\Delta\underline{\mathbf{r}}_{CF}$ in the CE frame, determined by integration over surface of sphere

$$\Delta\bar{\mathrm{r}}_{\mathrm{CF}} = \frac{1}{3}(h'_1 + 2l'_1)\mathbf{m}/M_{\oplus}$$

  - Use equations in CF frame in an inverse problem to estimate the parameters, equivalently
    - 3 degree-1 spherical harmonic coefficients
    - 3 components of the load moment vector

Degree-1 Deformations in Various Frames

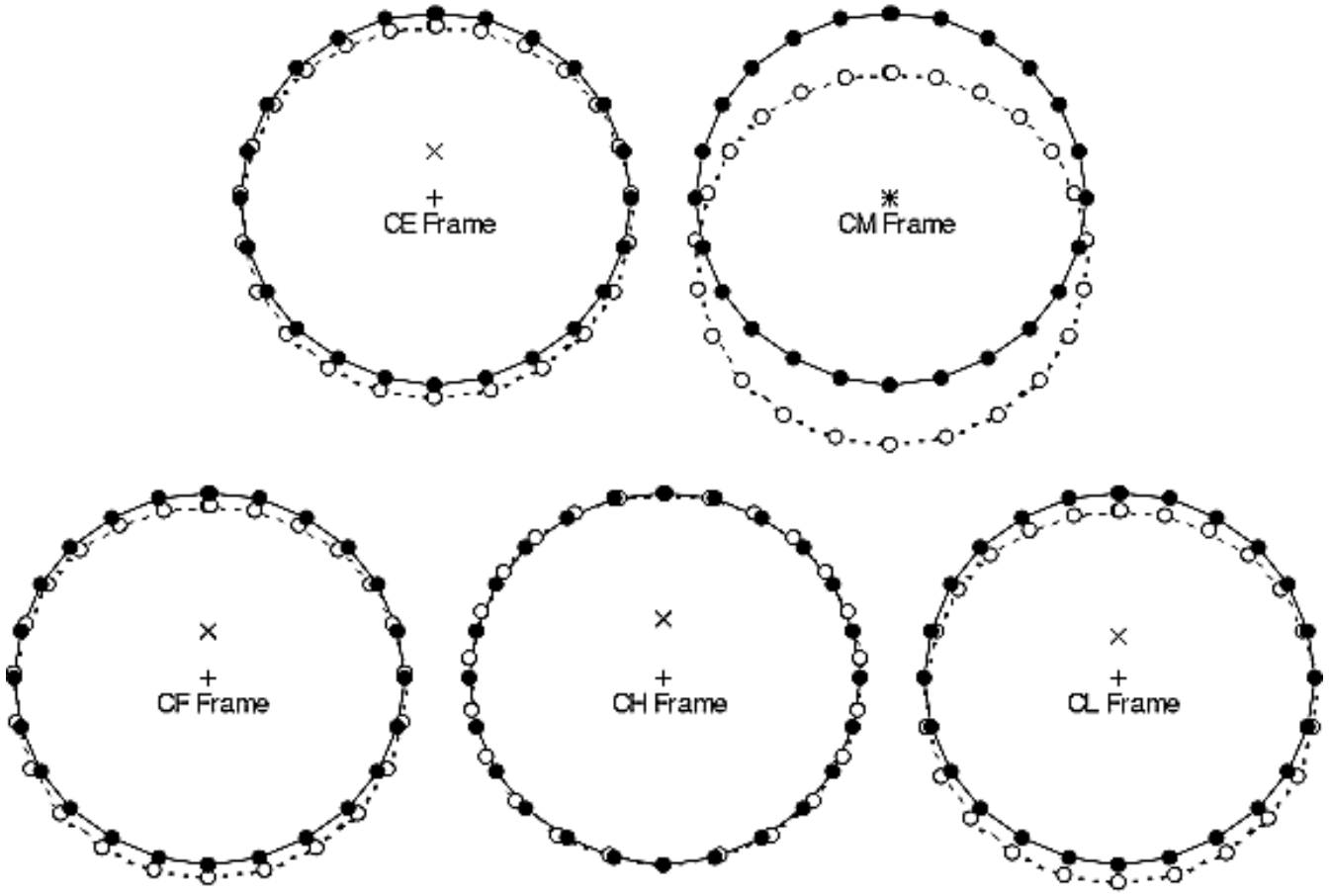

Blewitt (2003, JGR)

Results

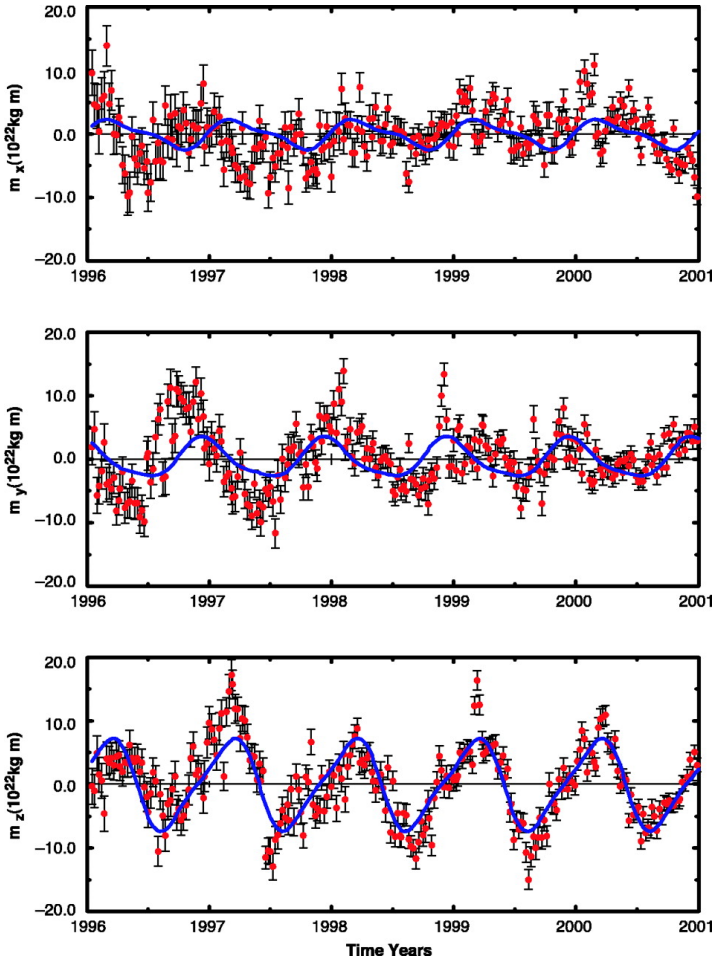
20.0
10.0
0.0
−10.0
−20.0
m x(10^22kg m)
m y(10^22kg m)
m z(10^22kg m)
1996
1997
1998
1999
2000
2001
Time Years

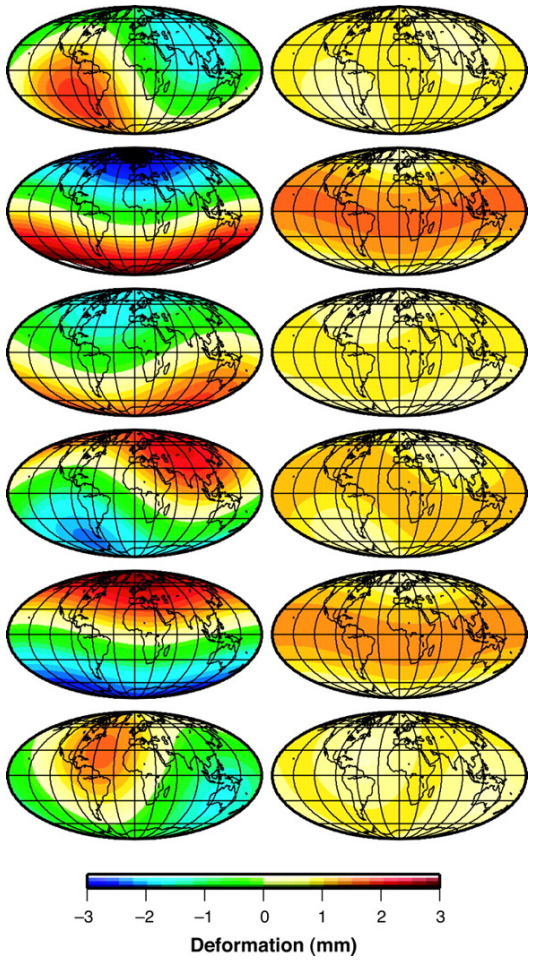
−3
−2
−1
0
1
2
3
Deformation (mm)

Results for Load Moment Vector

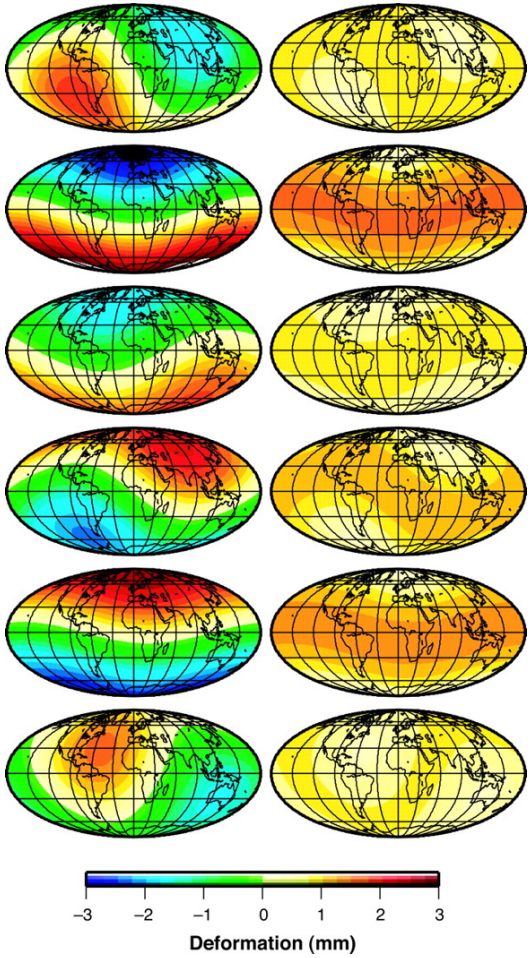

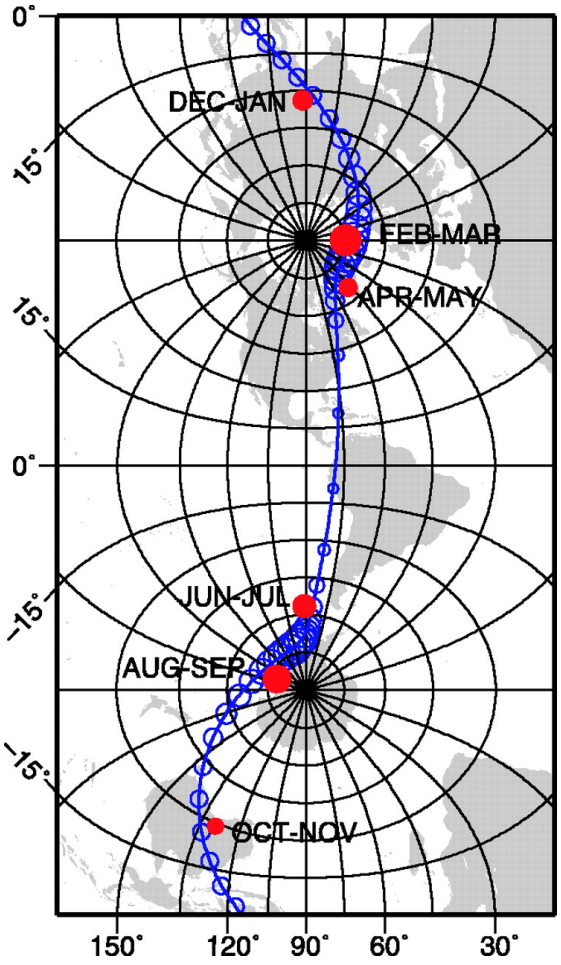

GPS Reflectometry

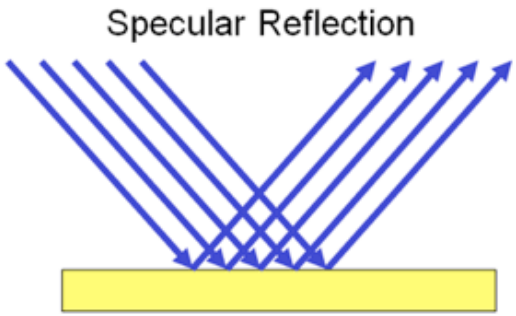

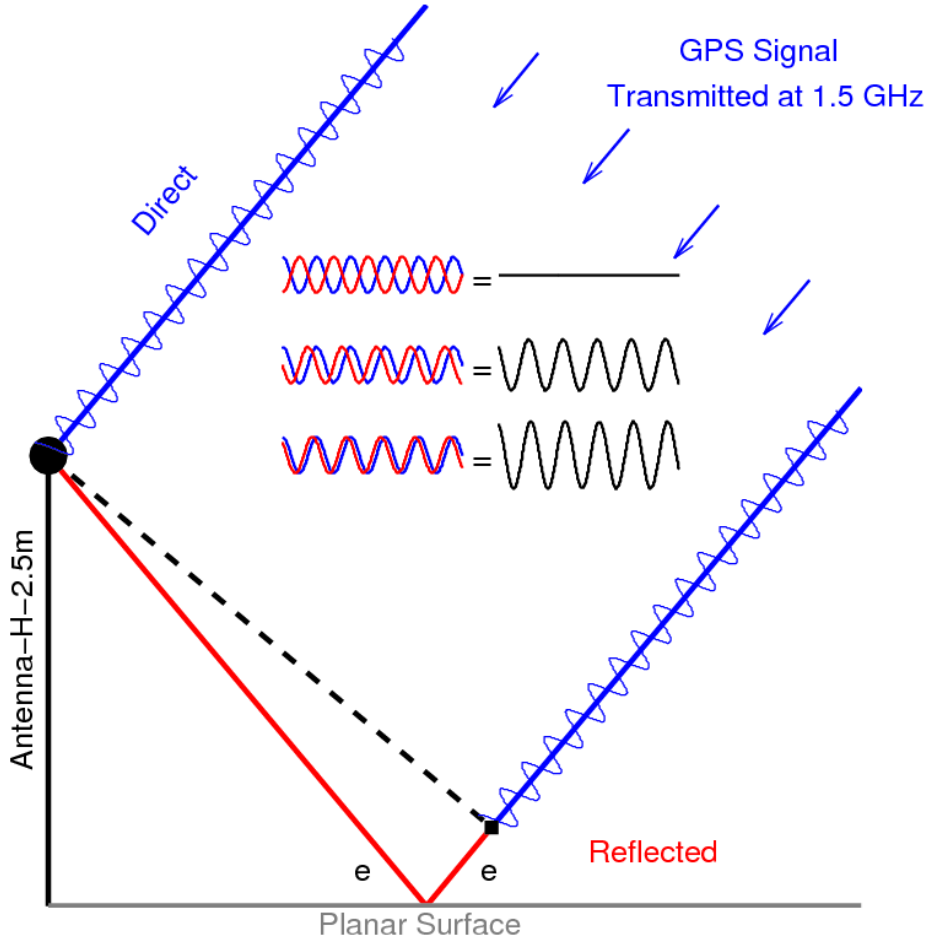

Kristine Larson, University of Colorado

Changes in Reflection Character

the reflections off bare soil produce this SNR curve

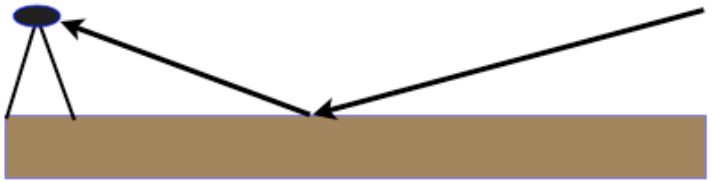

add a snow layer

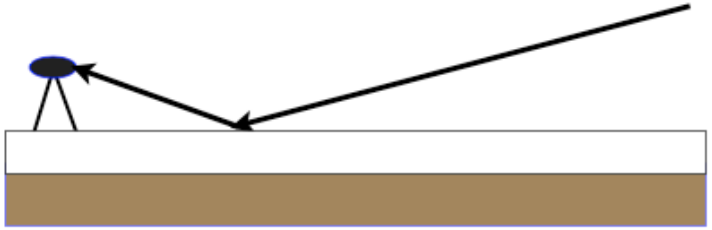

add vegetation

make the soil wet

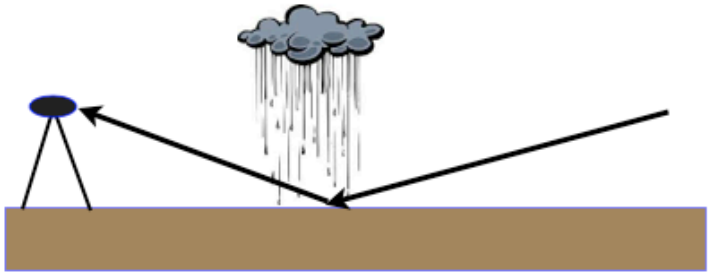

Kristine Larson, University of Colorado

GPS Reflectometry for Tides

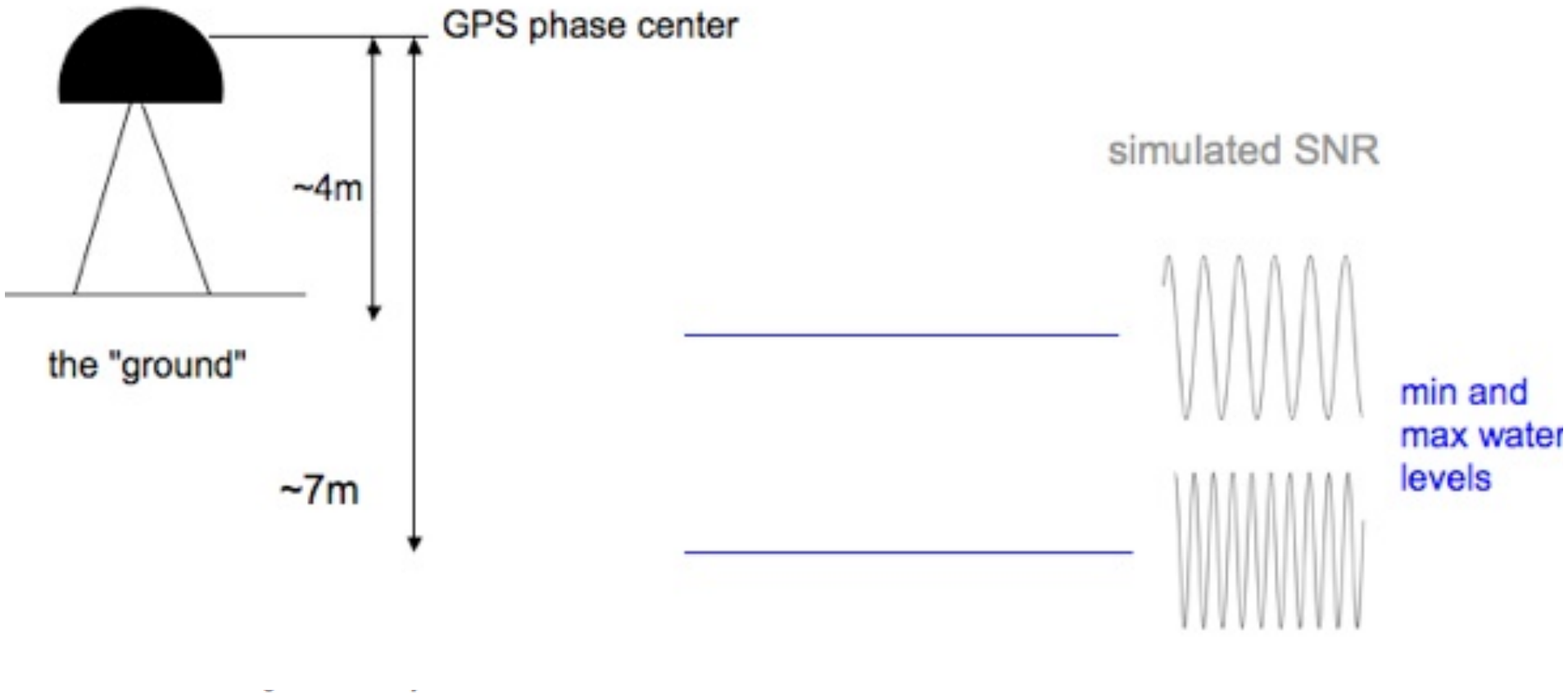

Kristine Larson, University of Colorado

Tide Gauge Example

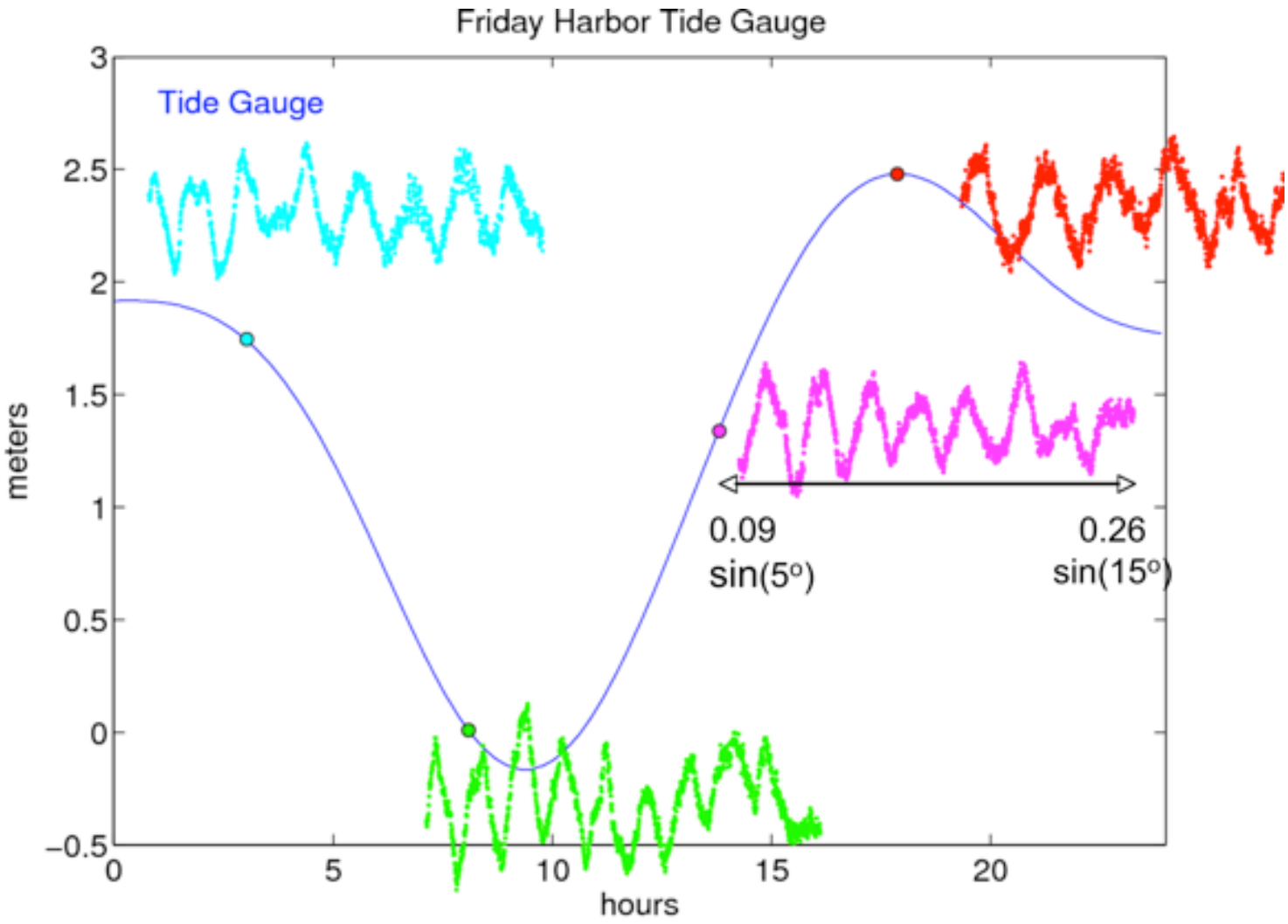

Larson et al. (2012)

Peterson Bay, Alaska

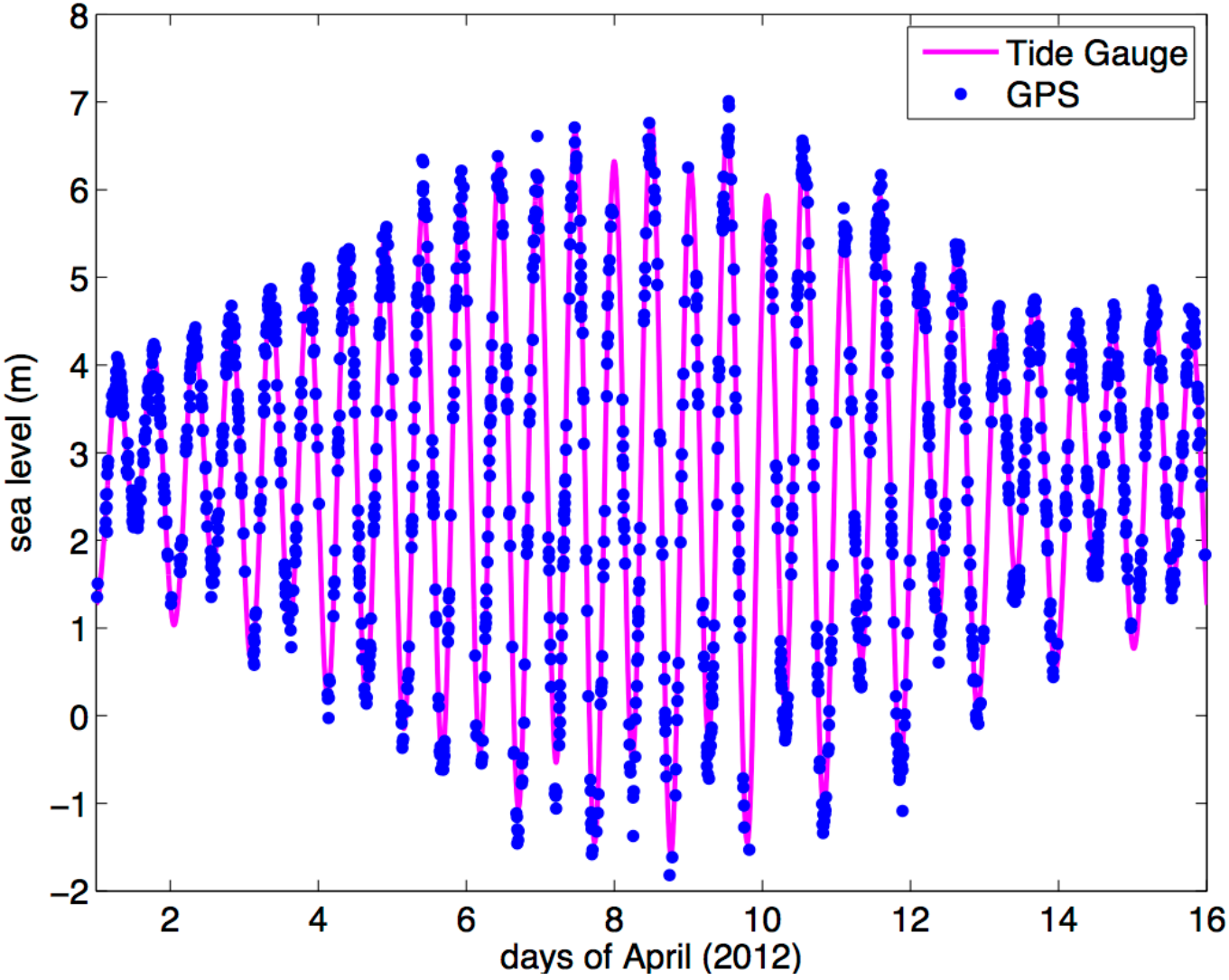

Larson et al. (2013)

Snow Depth

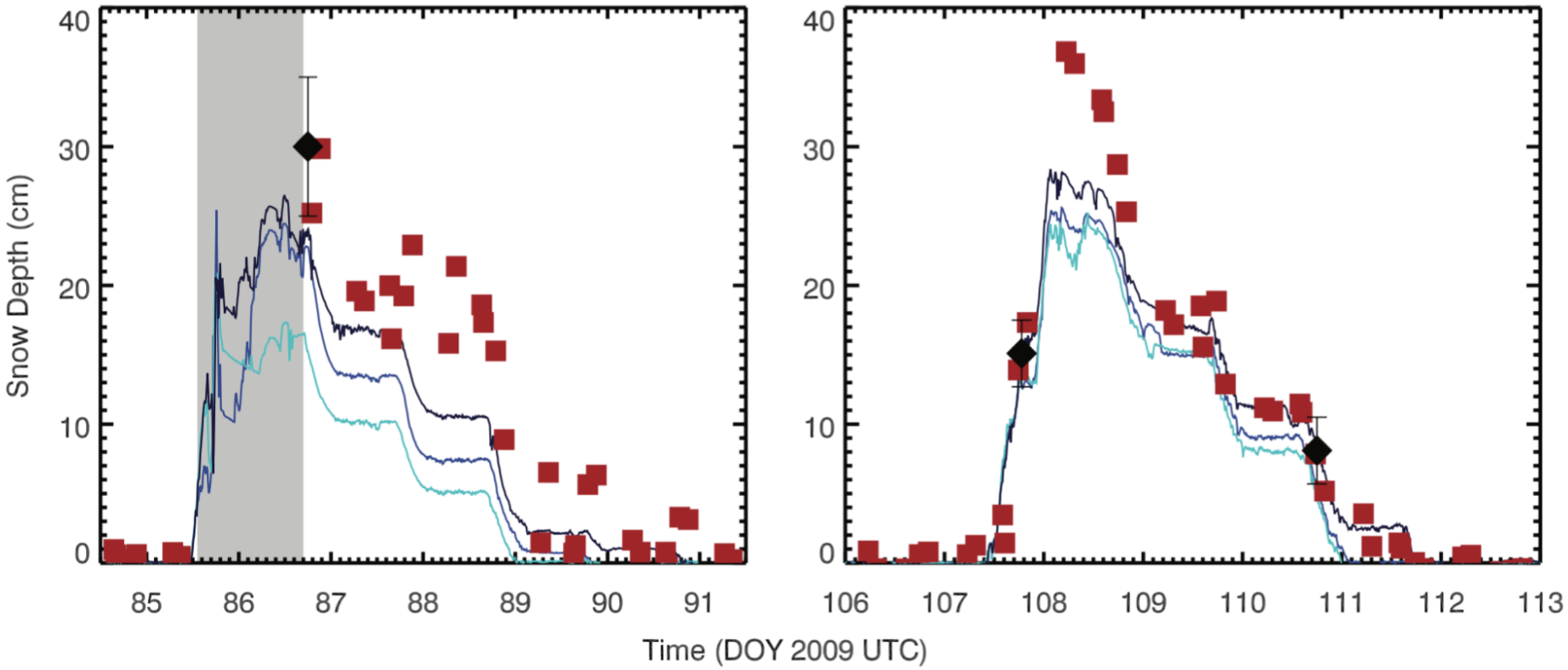

Larson et al. (2009)

Coldfoot Snow Depth 2016

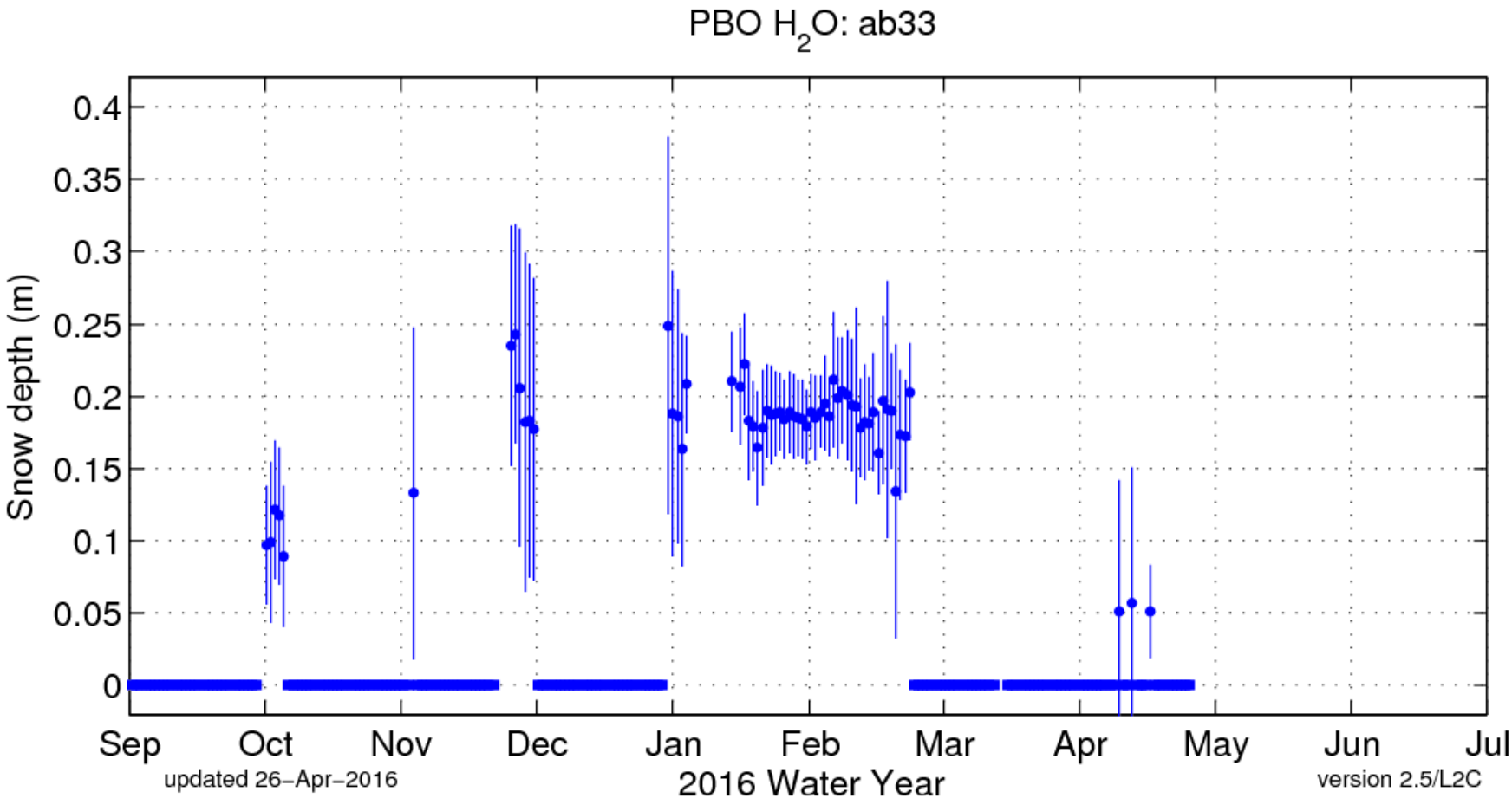

http://xenon.colorado.edu/portal/index.php?product=snow&station=ab33